

Data repository materials for Paleomagnetism of the Teel basalts from the Zavkhan Terrane: Implications for Paleozoic paleogeography in Mongolia and the growth of continental crust

Contents

1	Paleomagnetism of the Teel Formation	1
2	Teel Volcanics Data Analysis	1
2.1	Import Modules	2
2.2	Sampling localities	2
2.3	Site level data	4
2.4	Paleomagnetic site data summary	33
2.5	Paleomagnetic Poles for the Teel Formation	47
3	Pole compilation for Siberia, North China, and Mongolian terranes	64
3.1	Import existing paleomagnetic data	64
3.1.1	Siberia	64
3.1.2	North China	68
3.1.3	Mongolia pole compilation	70
3.2	Paleolatitude diagram	72
4	Regional overprints in Precambrian rocks	73
5	Data Repository References	77

1 Paleomagnetism of the Teel Formation

2 Teel Volcanics Data Analysis

This notebook is the data repository for a manuscript entitled:

Paleomagnetism of the Teel basalts from the Zavkhan Terrane: Implications for Paleozoic paleogeography in Mongolia and the growth of continental crust

T. M. Kilian, N. L. Swanson-Hysell, U. Bold, J. Crowley, and F. A. Macdonald

This manuscript is to be published in the GSA journal *Lithosphere*.

This notebook contains data analysis related to paleomagnetic data generated from basalt flows of the Late Ordovician Teel Formation from the Zavkhan Terrane. The underlying data are available both within the MagIC Database and in the GitHub repository association with this work: https://github.com/Swanson-Hysell-Group/2016_Teel_Basalts

2.1 Import Modules

Write template file (no_code.tplx) so that when the notebook is converted to latex (then pdf) it excludes the large code blocks. This requires an additional argument when using nbconveter and also requires that adding tables of content term after the document begins; can also add author. Can't include examples here because they affect the file when in latex.

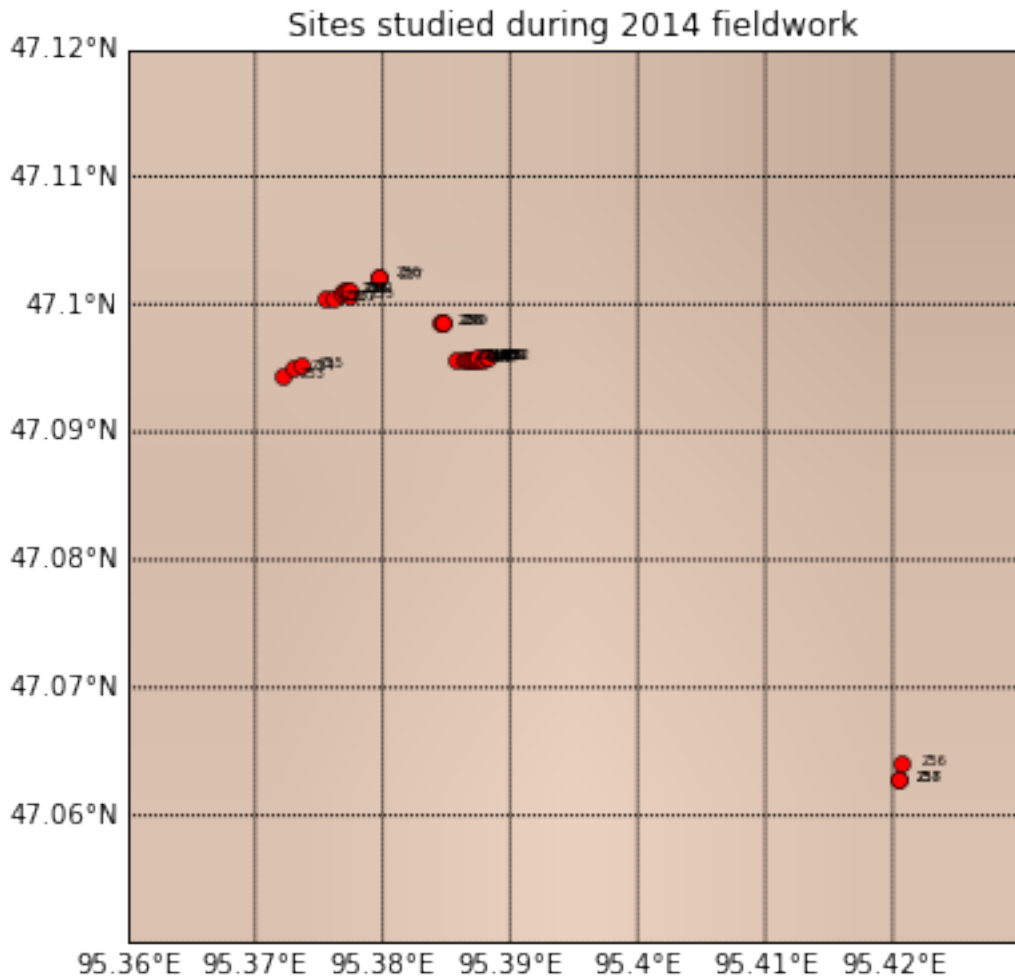
Overwriting no_code_latex.tplx

2.2 Sampling localities

Table of site locality coordinates given in WGS84 as well as a very simple map. Exact stratigraphic positions are shown in main text; order of stratigraphic position is given in “stat_pos” column of table. The paleomagnetic data from these sites may need to be tilt-corrected (depending on the age of magnetization) according to nearby measurements of bedding. The bedding tilts used for sites Z30 to Z55 come from interflow sedimentary rocks. The tilt-corrections for Z56 to Z58 are more uncertain and are based on interpreted flow banding.

Out [7] :

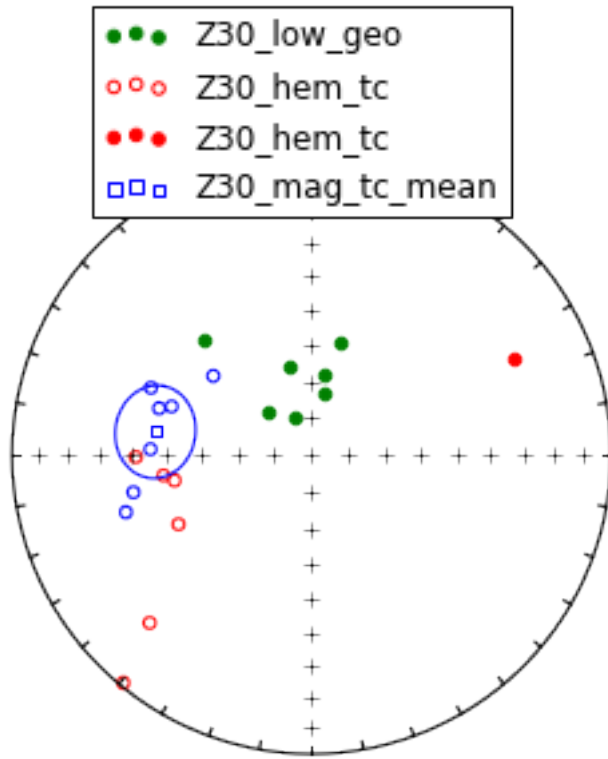
er_site_name	er_location_name	er_citation_names	site_class	site_definition	strat_pos	sample_bed_dip_direction	sample_bed_dip	site_lithology	site_lat	site_lon	site
0 Z30	Khukh_Davaa	This study	Extrusive	s	4.0	88	58	47.10038	Rhyolite	95.37550	Lava flow
1 Z31	Khukh_Davaa	This study	Extrusive	s	5.0	88	58	47.10049	Basalt	95.37604	Lava flow
2 Z32	Khukh_Davaa	This study	Extrusive	s	6.0	84	55	47.10094	Basalt	95.37684	Lava flow
3 Z33	Khukh_Davaa	This study	Extrusive	s	7.0	84	55	47.10107	Basalt	95.37705	Lava flow
4 Z34	Khukh_Davaa	This study	Extrusive	s	8.0	84	55	47.10111	Basalt	95.37712	Lava flow
5 Z35	Khukh_Davaa	This study	Extrusive	s	9.0	84	55	47.10069	Basalt	95.37747	Lava flow
6 Z36	Khukh_Davaa	This study	Extrusive	s	11.0	89	47	47.10221	Basalt	95.37859	Lava flow
7 Z37	Khukh_Davaa	This study	Extrusive	s	12.0	89	47	47.10211	Basalt	95.37971	Lava flow
8 Z38	Khukh_Davaa	This study	Extrusive	s	13.0	87	46	47.09855	Basalt	95.38445	Lava flow
9 Z39	Khukh_Davaa	This study	Extrusive	s	14.0	87	46	47.09860	Basalt	95.38467	Lava flow
10 Z40	Khukh_Davaa	This study	Extrusive	s	15.0	87	46	47.09859	Basalt	95.38474	Lava flow
11 Z41	Khukh_Davaa	This study	Extrusive	s	10.0	84	55	47.10109	Basalt	95.37744	Lava flow
12 Z42	Khukh_Davaa	This study	Extrusive	s	16.0	87	37	47.09577	Basalt	95.38577	Lava flow
13 Z43	Khukh_Davaa	This study	Extrusive	s	17.0	87	37	47.09570	Basalt	95.38638	Lava flow
14 Z44	Khukh_Davaa	This study	Extrusive	s	18.0	87	37	47.09571	Basalt	95.38651	Lava flow
15 Z45	Khukh_Davaa	This study	Extrusive	s	19.0	87	37	47.09562	Basalt	95.38676	Lava flow
16 Z46	Khukh_Davaa	This study	Extrusive	s	20.0	87	37	47.09563	Basalt	95.38692	Lava flow
17 Z47	Khukh_Davaa	This study	Extrusive	s	21.0	87	37	47.09568	Basalt	95.38727	Lava flow
18 Z48	Khukh_Davaa	This study	Extrusive	s	22.0	91	28	47.09570	Basalt	95.3874	Lava flow
19 Z49	Khukh_Davaa	This study	Extrusive	s	23.0	91	28	47.09581	Basalt	95.38747	Lava flow
20 Z50	Khukh_Davaa	This study	Extrusive	s	24.0	91	28	47.09575	Basalt	95.38781	Lava flow
21 Z51	Khukh_Davaa	This study	Extrusive	s	25.0	91	28	47.09584	Basalt	95.38802	Lava flow
22 Z52	Khukh_Davaa	This study	Extrusive	s	26.0	91	28	47.09583	Basalt	95.38815	Lava flow
23 Z53	Khukh_Davaa	This study	Extrusive	s	1.0	88	58	47.09442	Basalt	95.37205	Lava flow
24 Z54	Khukh_Davaa	This study	Extrusive	s	2.0	88	58	47.09502	Basalt	95.37299	Lava flow
25 Z55	Khukh_Davaa	This study	Extrusive	s	3.0	88	58	47.09525	Basalt	95.37351	Lava flow
26 Z56	Khukh_Davaa	This study	Extrusive	s	NaN	24	47.06403	Basalt	95.42039	Lava flow	
27 Z57	Khukh_Davaa	This study	Extrusive	s	NaN	24	47.06277	Basalt	95.42039	Lava flow	
28 Z58	Khukh_Davaa	This study	Extrusive	s	NaN	24	47.06277	Basalt	95.42045	Lava flow	



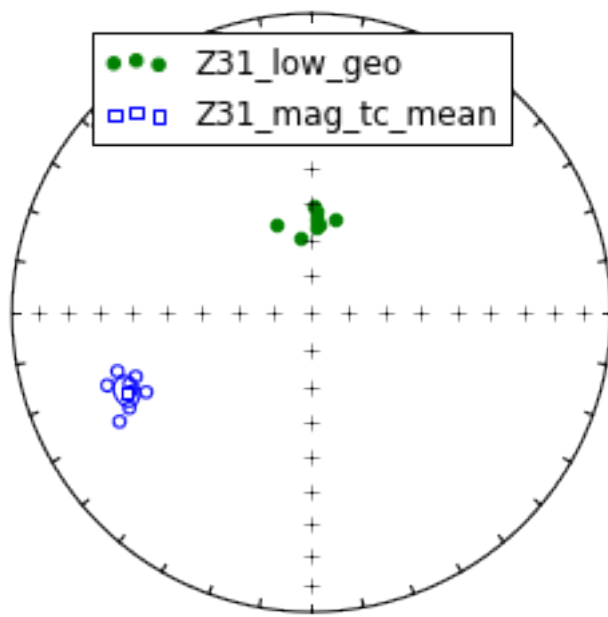
2.3 Site level data

Below we import paleomagnetic results that were analyzed using demag_gui.py from the PmagPy python package. These are the vector component fits to all Teel sample data. Components have been classified according to their relative temperature ranges. ‘LOW’ components are typically below 200°C, ‘MAG’ refers to a temperature range within the unblocking range of magnetite (up to 580°C), ‘HEM’ refers to vector components fit to data points in the unblocking range of hematite (up to 680°C), and ‘MID’ refers to components with temperature ranges between ‘LOW’ and ‘MAG’.

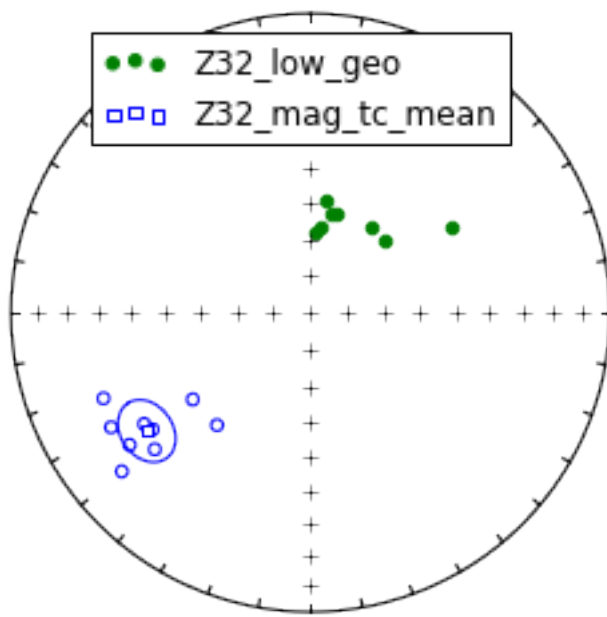
Z30 Site Z30 is a rhyolite. The site has ‘LOW’, ‘MAG’ and poorly resolved ‘HEM’ components.



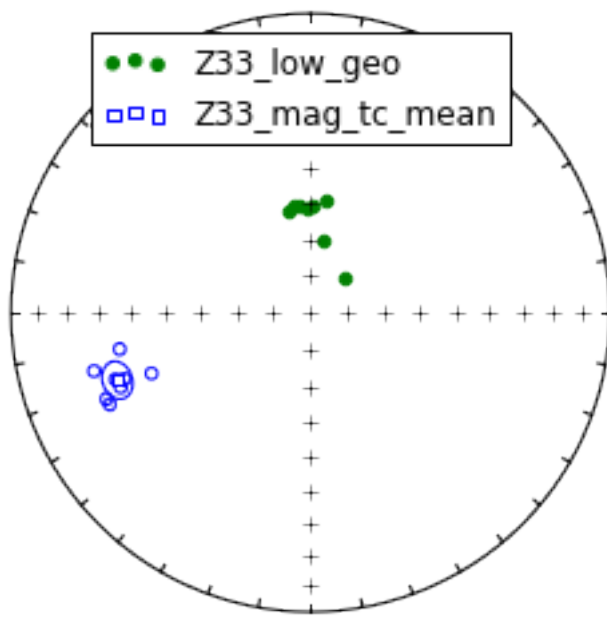
Z31 The site has 'LOW' (less than 200°C) and 'MAG' components.



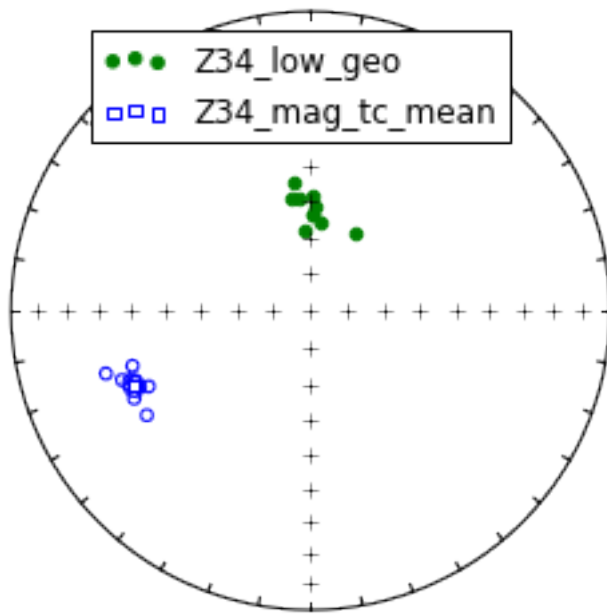
Z32 The site has 'LOW' (less than 200°C) and 'MAG' components.



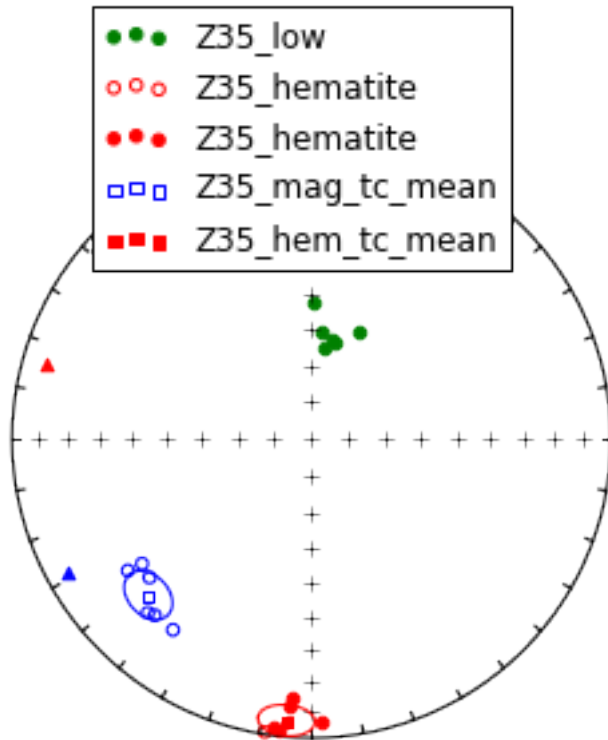
Z33 The site has 'LOW' (less than 200°C) and 'MAG' components.



Z34 The site has 'LOW' (less than 200°C) and 'MAG' components.

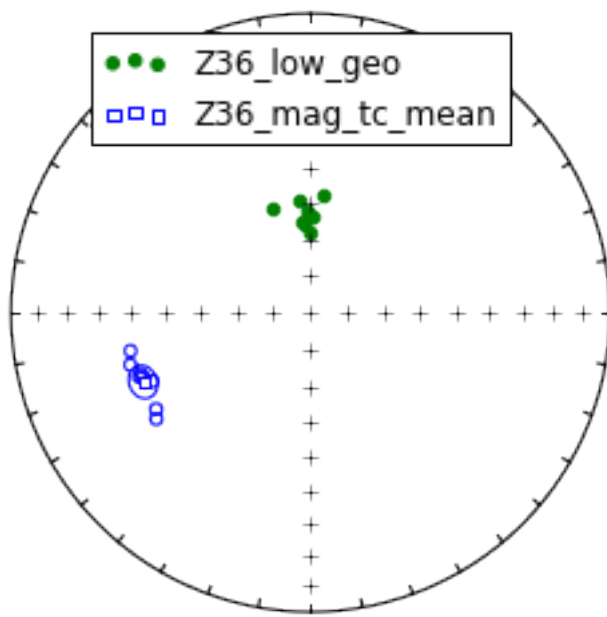


Z35 The site has 'LOW', 'MAG' and 'HEM' components.

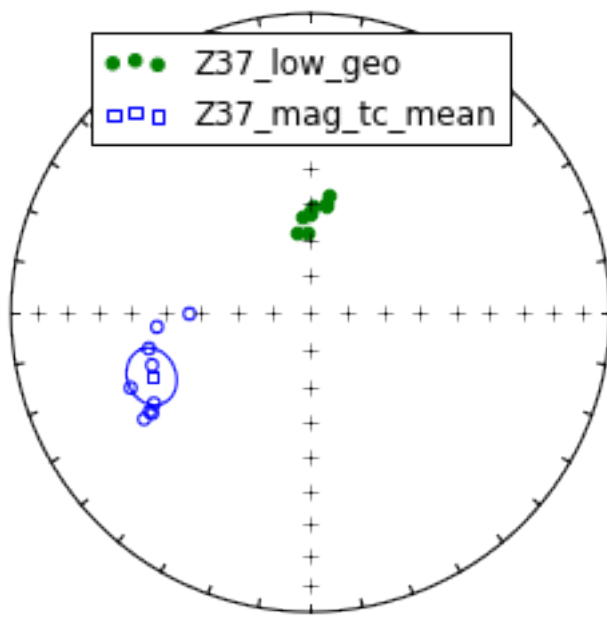


Data points shown with triangles were vectors from sample Z35.3 that were dropped from the mean calculation.

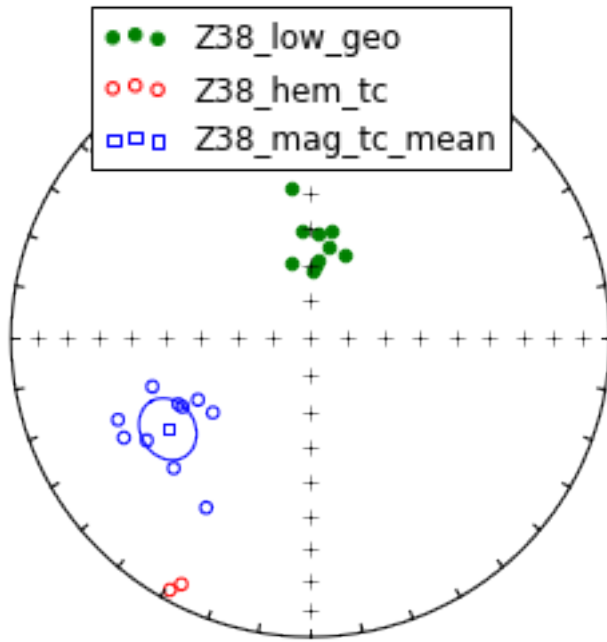
Z36 The site has 'LOW' and 'MAG' components.



Z37 The site has ‘LOW’ and ‘MAG’ components.

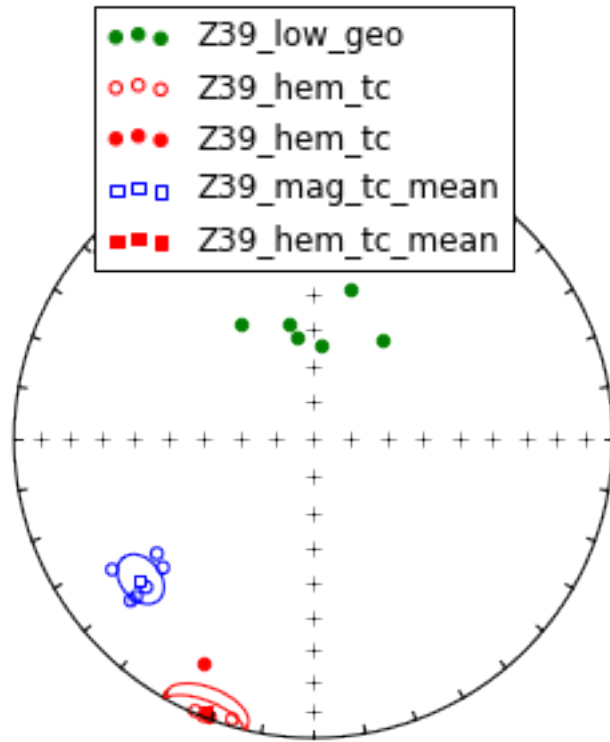


Z38 The site has 'LOW', 'MAG' and 'HEM' components.

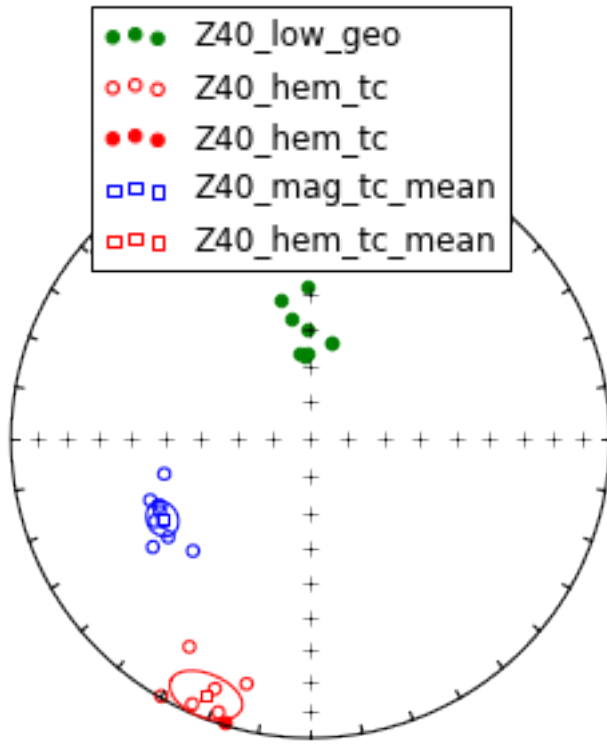


Only two samples yielded hematite components, therefore no mean was calculated for the hematite component.

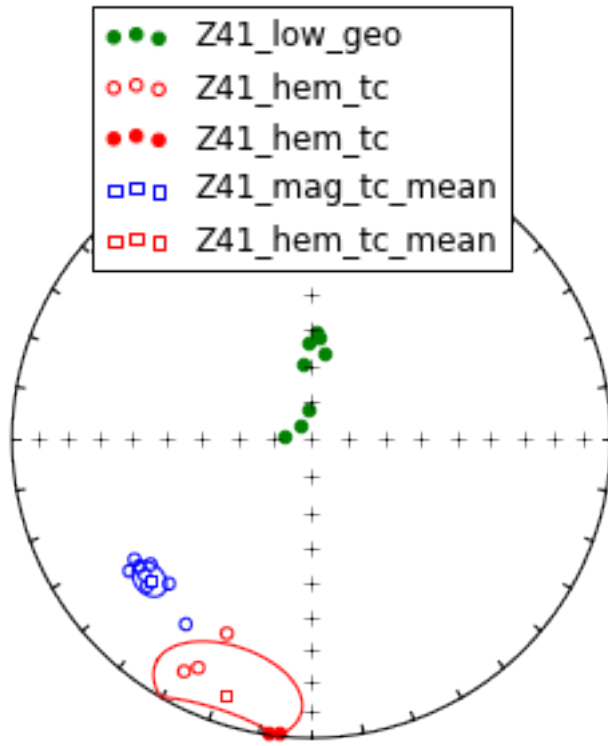
Z39 The site has ‘LOW’, ‘MAG’ and ‘HEM’ components.



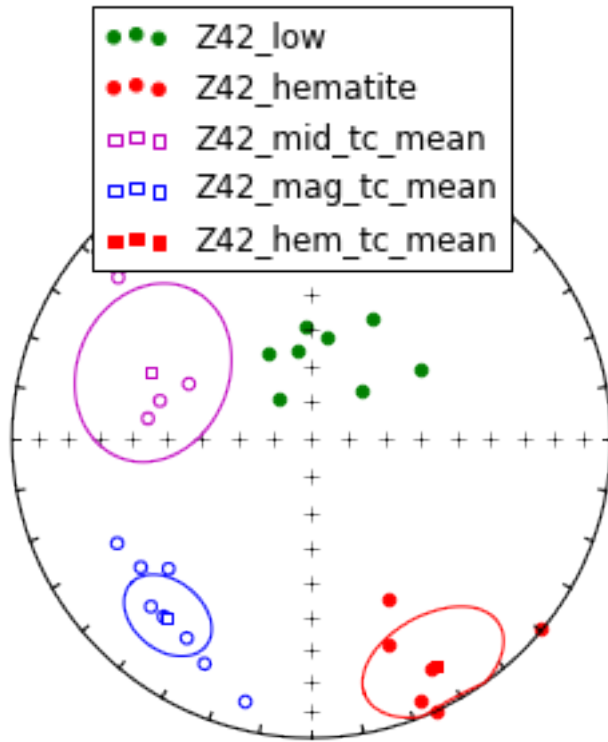
Z40 The site has ‘LOW’, ‘MAG’ and ‘HEM’ components.



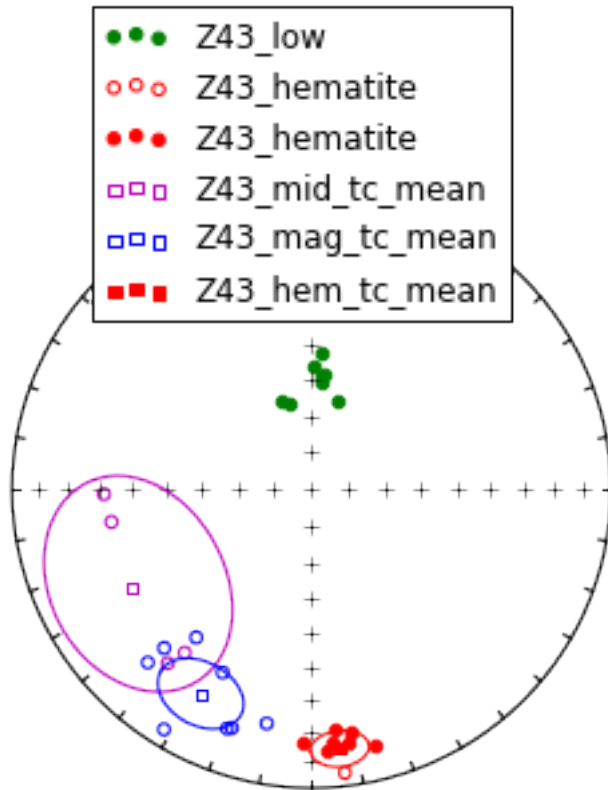
Z41 The site has ‘LOW’, ‘MAG’ and ‘HEM’ components.



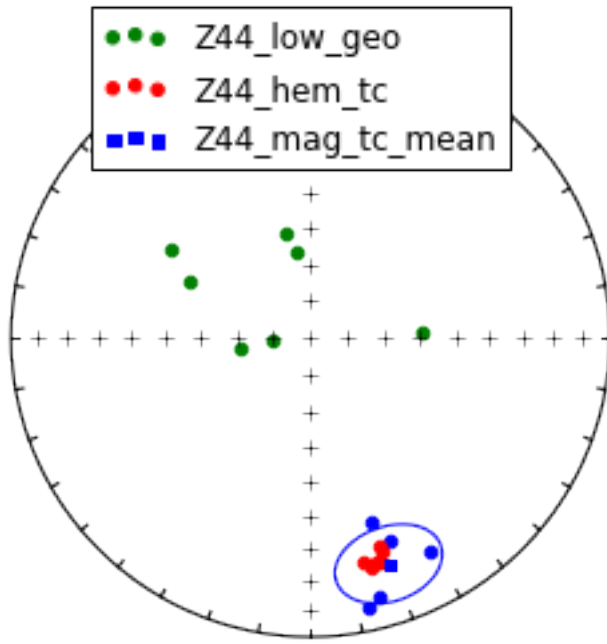
Z42 The site has ‘LOW’, ‘MAG’ and ‘HEM’ components. A middle temperature component, MID, was also fit to demagnetization steps between ‘LOW’ and ‘MAG’.



Z43 The site has ‘LOW’, ‘MAG’ and ‘HEM’ components. A middle temperature component, MID, was also fit to demagnetization steps between ‘LOW’ and ‘MAG’.

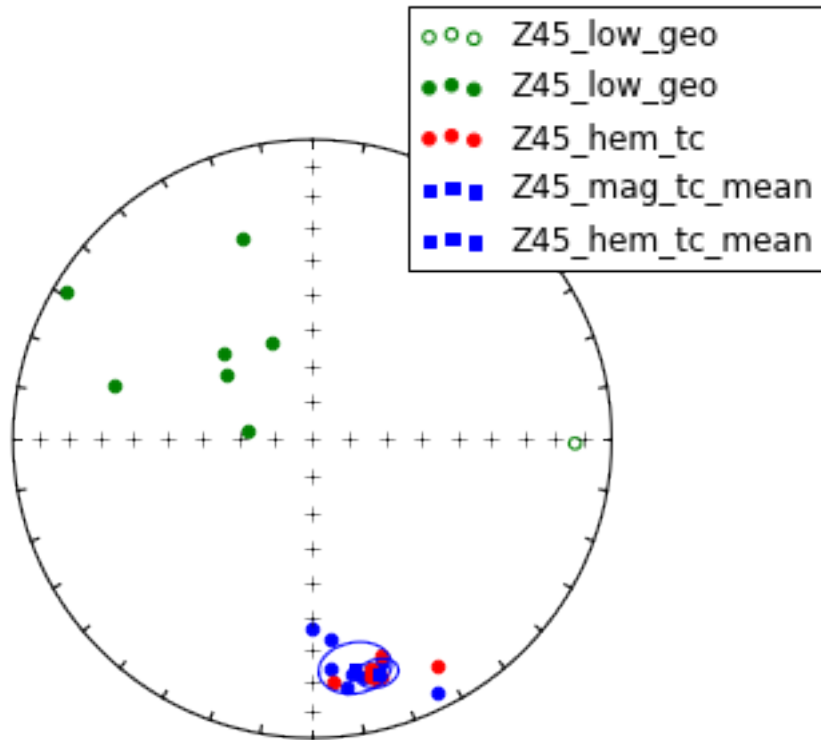


Z44 The site has 'LOW', 'MAG' and 'HEM' components.



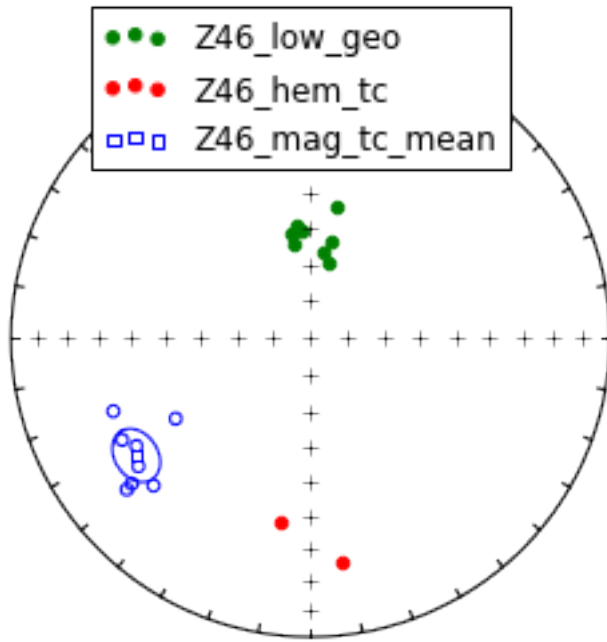
The remanence of Z44 specimens is dominated by hematite such that the magnetite component is poorly resolved.

Z45 Hematite, magnetite, and low temperature, LOW (less than 200°C), components were calculated for Z45.

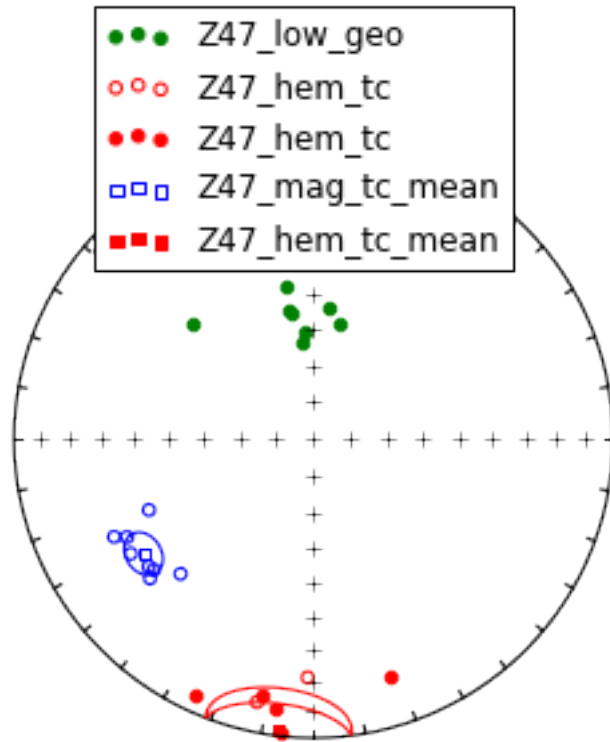


The remanence of Z45 specimens is dominated by hematite such that the magnetite component is poorly resolved.

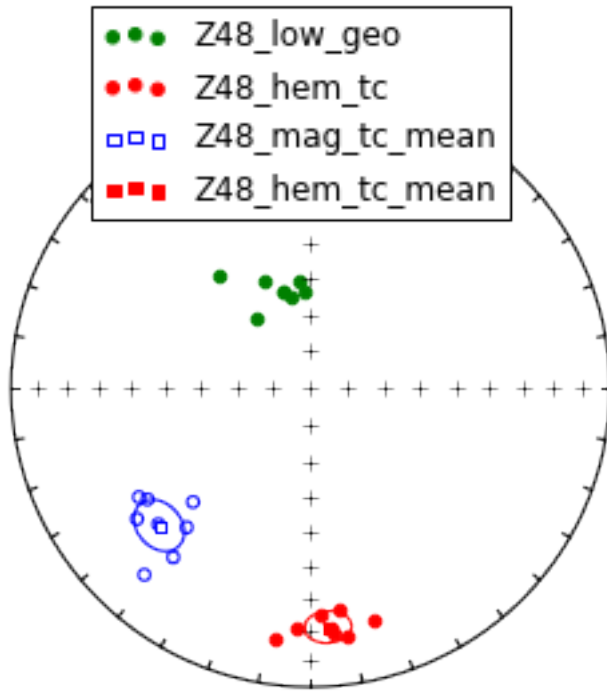
Z46 The site has ‘LOW’, ‘MAG’ and ‘HEM’ components.



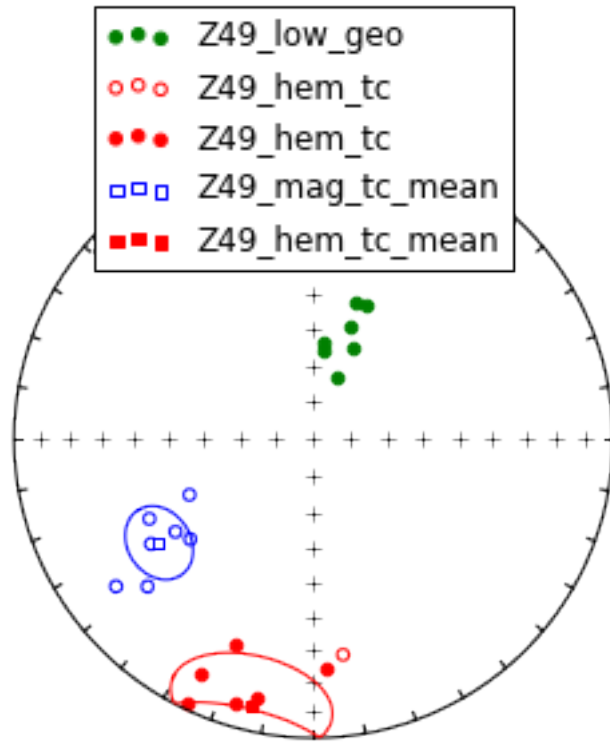
Z47 The site has 'LOW', 'MAG' and 'HEM' components.



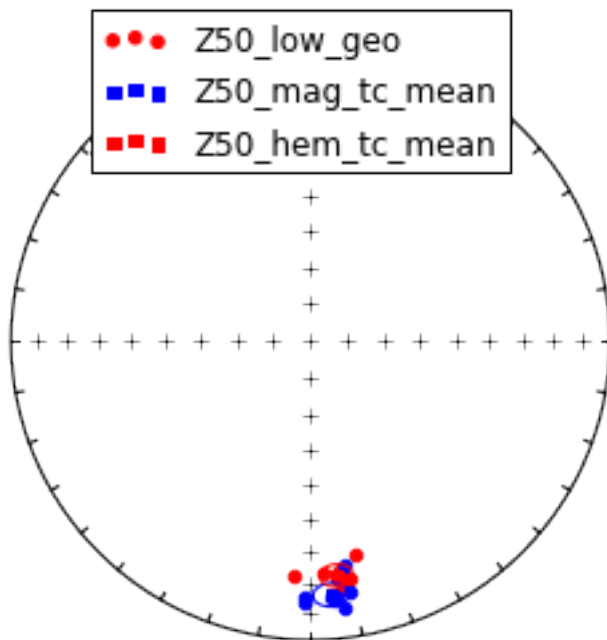
Z48 The site has ‘LOW’, ‘MAG’ and ‘HEM’ components.



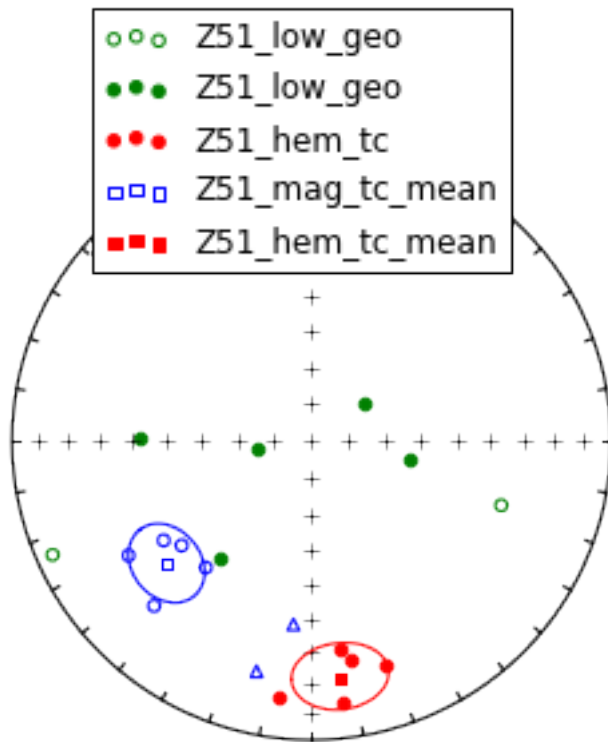
Z49 The site has 'LOW', 'MAG' and 'HEM' components.



Z50 The site has ‘MAG’ and ‘HEM’ components.

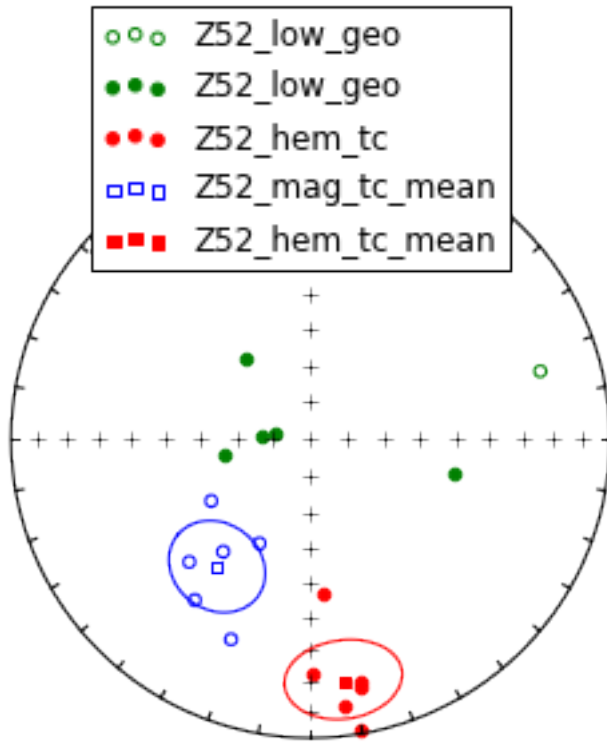


Z51 The site has 'LOW', 'MAG' and 'HEM' components.

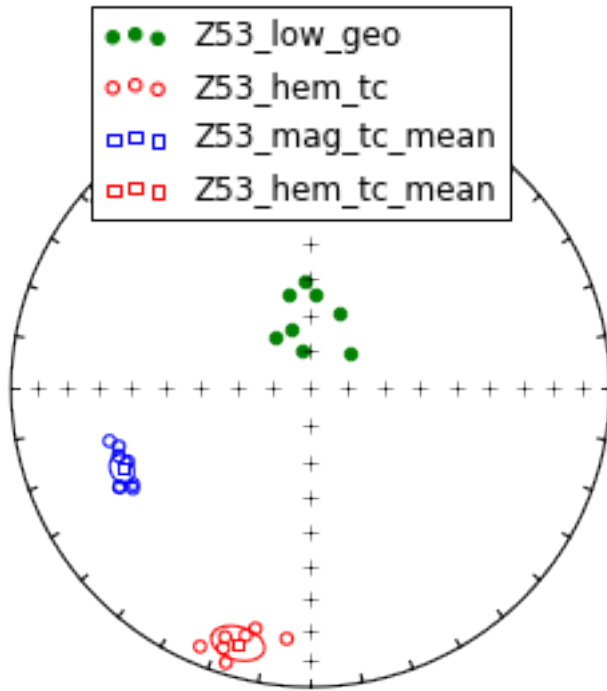


Magnetite components from two samples (Z51.1 and Z51.2) were excluded because of their similarity to hematite components (the hematite remanence mixed with that of magnetite) and different demagnetization behavior compared to the other magnetite components.

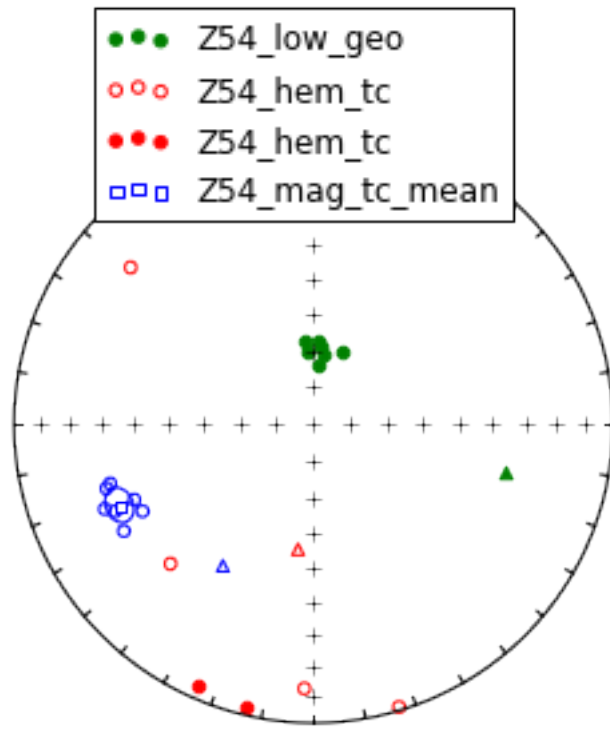
Z52 The site has ‘LOW’, ‘MAG’ and ‘HEM’ components.



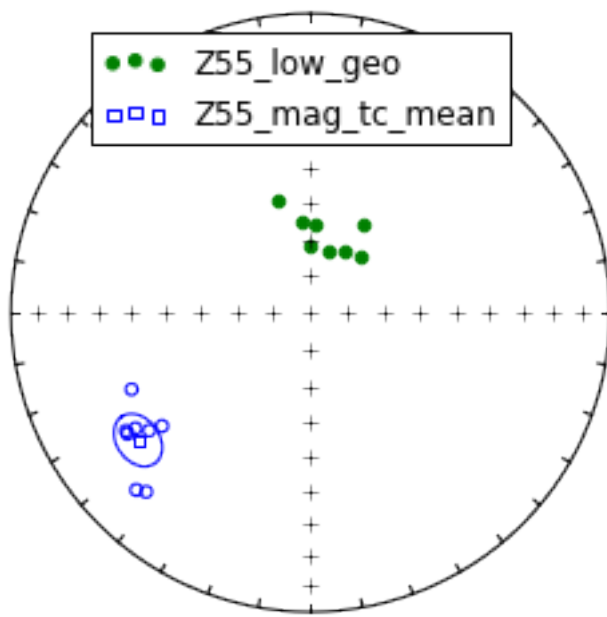
Z53 The site has ‘LOW’, ‘MAG’ and ‘HEM’ components.



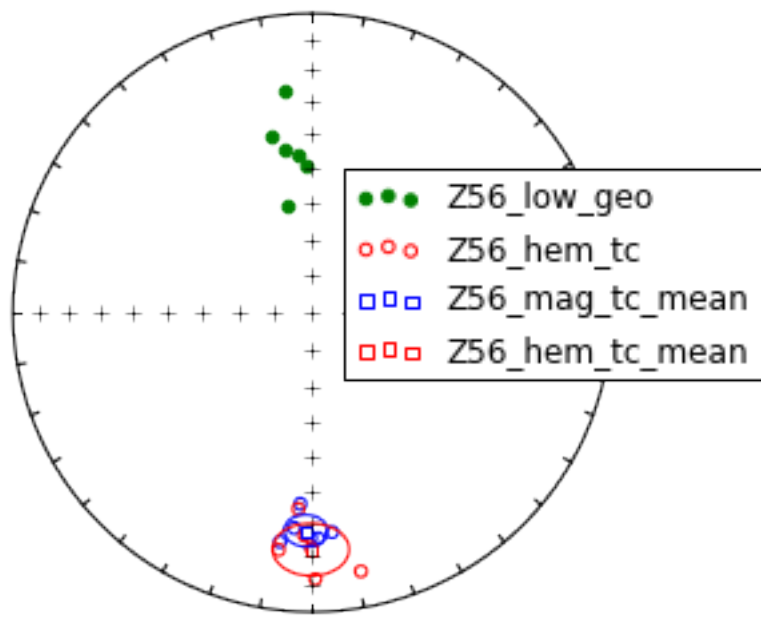
Z54 The site has 'LOW', 'MAG' and 'HEM' components.



Z55 The site has 'LOW' and 'MAG'.

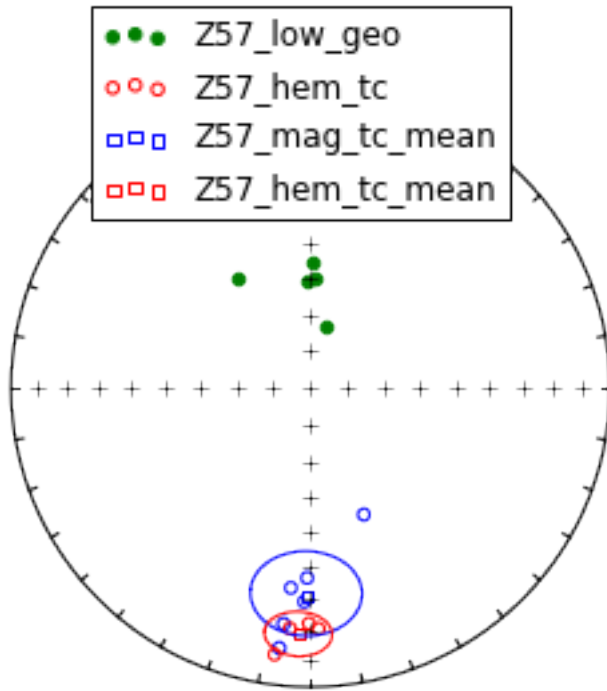


Z56 The site has 'LOW', 'MAG' and 'HEM' components.

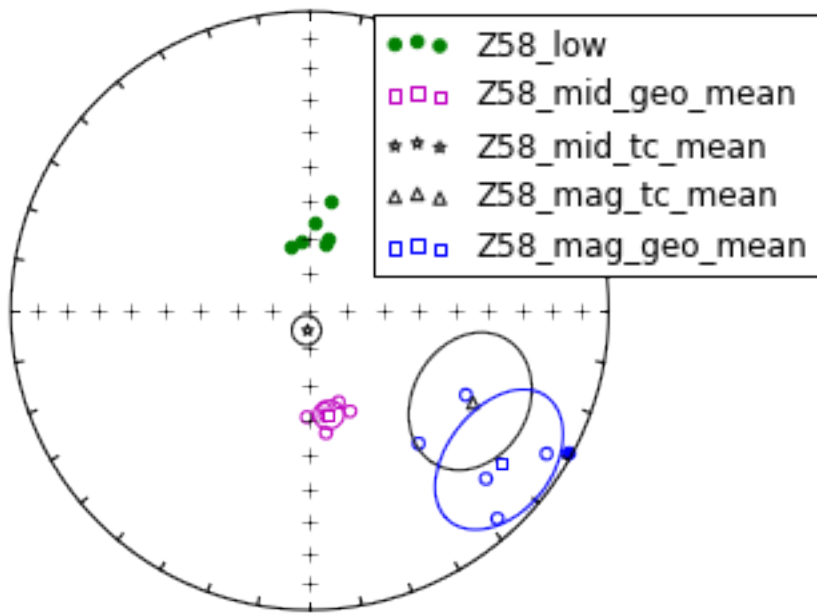


This site is in a different dip panel along with Z57 and Z58. A magnetite component distinct from the hematite component was not resolved. Z57 has similar behavior.

Z57 The site has ‘LOW’, ‘MAG’ and ‘HEM’ components.



Z58 Magnetite, mid-, and low- temperature, LOW (less than 200°C), components were calculated for Z58. The middle temperature component derives from demagnetization steps between LOW and magnetite.



Results from flow Z58 are very different from all of the other sites.

2.4 Paleomagnetic site data summary

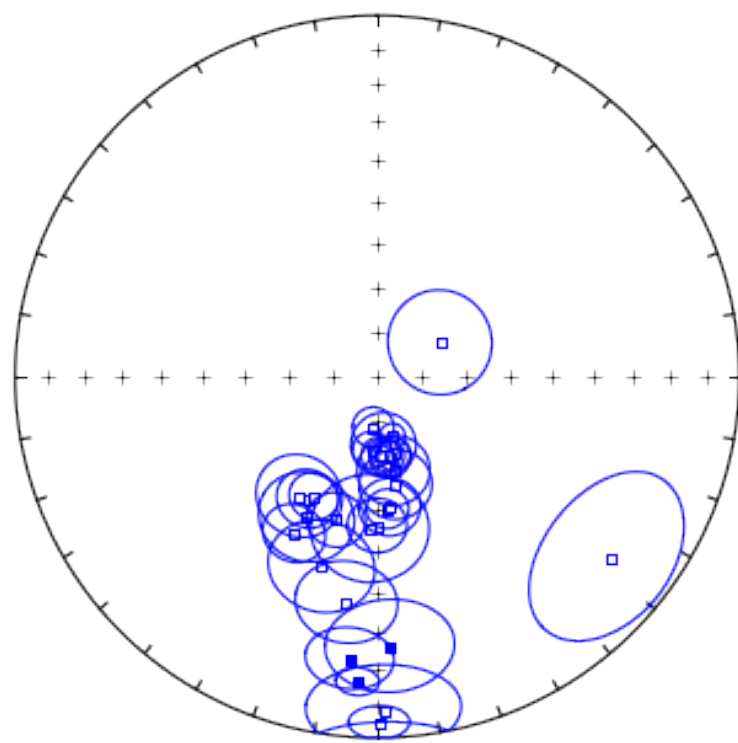
Create tables, distinguished by component type, of mean directions for all Teel flows.

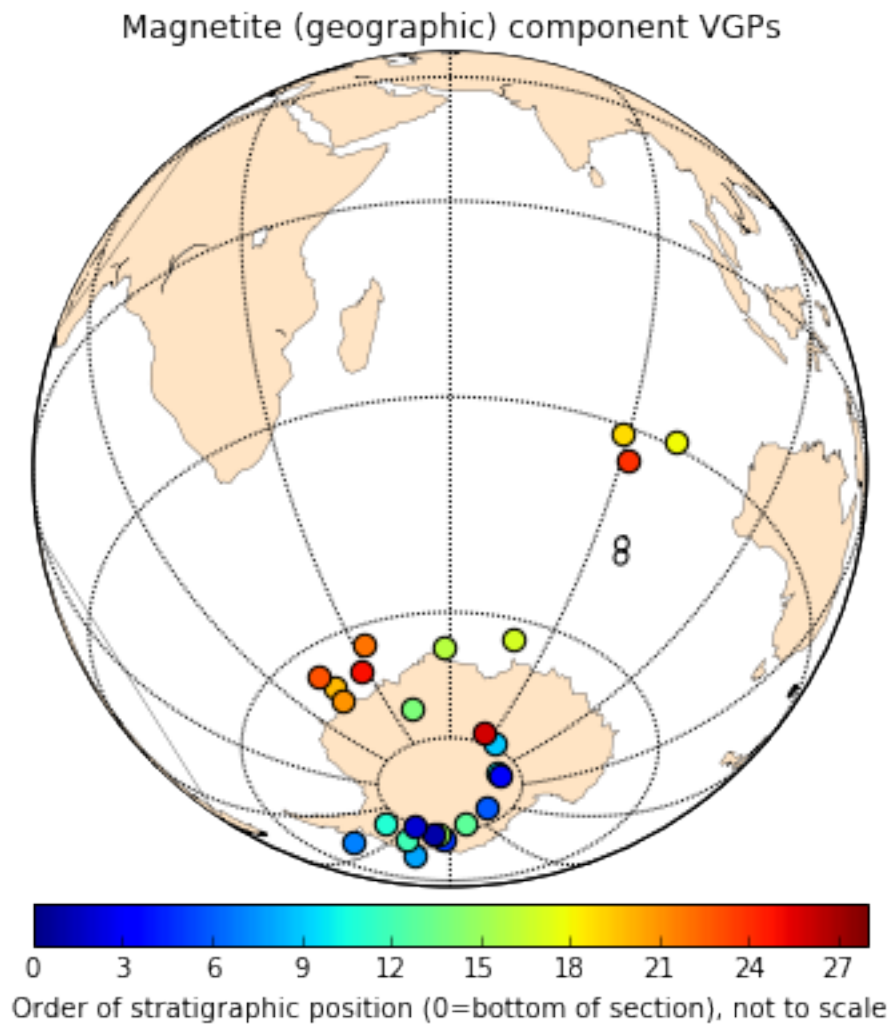
Magnetite directions

Geographic coordinates - magnetite Out[68]:

	strat_pos	site_lat	site_lon	dec_geo	inc_geo	alpha95	n	k	r	cstd	paleolatitude	vgp_lat	vgp_lon	vgp_lat_rev	vgp_lon_rev
Z30	mag_geo	4.0	47.10038	95.37530	61.199035	-73.861110	11.712582	7	27.513985	6.781929	15.442168	-59.940264	-28.018244	245.553956	28.018244
Z31	mag_geo	5.0	47.10049	95.37664	168.10323	-72.234668	3.753459	8	218.756351	7.968001	5.476520	-57.348450	-77.463763	244.552326	64.463763
Z32	mag_geo	6.0	47.10094	95.37684	170.358327	-65.228366	7.987595	9	42.504477	8.811785	12.424178	-47.295204	-83.450449	190.612182	63.450449
Z33	mag_geo	7.0	47.10107	95.37705	184.611118	4.579774	8	147.251468	7.952462	6.675060	-68.002034	-68.966892	280.18909	68.966892	
Z34	mag_geo	8.0	47.10111	95.37712	165.710554	-76.241270	2.846954	10	288.897760	9.968847	4.765549	-63.908090	-71.445651	255.430852	71.445651
Z35	mag_geo	9.0	47.10069	95.37747	180.03525	-56.117492	6.392221	6	110.823428	5.954583	7.694302	-36.670242	-79.569519	79.569519	75.19636
Z36	mag_geo	11.0	47.10221	95.37959	184.602274	-73.486350	4.160116	8	178.256339	7.960731	6.066839	-59.330331	-77.472330	286.256471	77.472330
Z37	mag_geo	12.0	47.10211	95.37971	174.776055	-74.649777	7.228282	9	51.767913	8.845464	11.257830	-61.232208	-75.554119	265.265069	75.554119
Z38	mag_geo	13.0	47.09855	95.38445	170.143849	-68.504682	8.040139	10	37.061501	9.757160	13.305265	-51.774894	-82.077055	225.173390	82.077055
Z39	mag_geo	14.0	47.09860	95.38467	196.103583	-56.02026	6.360400	6	111.925588	5.955527	7.656324	-36.571555	-74.094885	241.094885	241.094885
Z40	mag_geo	15.0	47.09859	95.38474	170.919387	-71.617755	4.526930	9	130.309345	8.938608	7.095733	-56.391067	-79.159498	247.707629	79.159498
Z41	mag_geo	16.0	47.10109	95.37744	175.528998	-59.942821	4.580179	8	147.225628	7.952454	6.675646	-40.828095	-82.952076	124.113660	82.952076
Z42	mag_geo	16.0	47.09877	95.38692	196.391432	-44.308602	11.150650	8	25.632057	7.726904	15.999017	-26.015890	-65.235979	58.083778	248.235979
Z43	mag_geo	17.0	47.09570	95.38638	187.775559	-36.897405	10.300671	8	29.872943	7.765674	14.819925	-20.574890	-62.736797	79.335353	29.335353
Z44	mag_geo	18.0	47.09571	95.38651	177.320106	25.95966	12.330351	5	39.443485	8.898589	12.897258	13.677537	-29.179269	98.369133	27.4179269
Z45	mag_geo	19.0	47.09562	95.38676	185.597011	22.580727	8.288935	8	45.635763	7.846612	11.990364	11.751342	-30.940533	88.994843	30.940533
Z46	mag_geo	20.0	47.09563	95.38692	209.756875	-58.037356	6.730898	8	68.683122	7.890803	9.773723	-38.706221	-66.816385	15.707150	66.816385
Z47	mag_geo	21.0	47.09568	95.38727	207.834821	-59.308788	5.435421	8	104.816159	7.933216	7.911720	-40.110460	-68.801903	14.424098	14.424098
Z48	mag_geo	22.0	47.09570	95.38744	207.921657	-49.34542	6.769918	8	68.082983	7.897184	9.816705	-30.295949	-62.672462	33.563559	62.672462
Z49	mag_geo	23.0	47.09581	95.38747	213.177701	-57.526629	9.488165	7	41.429419	6.855175	12.584345	-38.154890	-64.234334	13.523120	64.234334
Z50	mag_geo	24.0	47.09575	95.38781	183.717558	16.532802	3.910452	8	201.619149	7.965281	5.704520	8.442107	-34.363744	90.931921	27.221921
Z51	mag_geo	25.0	47.09584	95.38802	206.717692	-54.030732	10.393892	5	55.146896	4.927466	10.907481	-34.565590	-66.394972	27.782142	66.394972
Z52	mag_geo	26.0	47.09583	95.38815	182.885182	-55.213178	12.719642	6	28.697188	5.825767	15.120472	-35.744789	-78.453731	83.817965	263.177965
Z53	mag_geo	1.0	47.09442	95.37205	172.274867	-71.983776	3.594132	8	238.494787	7.970649	5.245001	-56.957385	-79.068440	252.646197	79.068440
Z54	mag_geo	2.0	47.09502	95.37299	177.77554	-72.215892	4.246460	7	203.040657	6.970449	5.684516	-57.319102	-79.686885	268.650137	79.686885
Z55	mag_geo	3.0	47.09525	95.37351	174.593057	-60.266013	6.693178	8	69.448675	7.899206	9.719704	-41.198461	-62.944253	130.647847	82.944253
Z56	mag_geo	NaN	47.06403	95.42075	179.680351	-4.756236	5.057226	6	176.489683	5.971670	6.097129	-45.317329	-55.874466	95.874936	45.317329
Z57	mag_geo	NaN	47.06277	95.42045	178.924941	-8.201891	13.191510	6	26.747477	5.813066	15.661870	-4.122063	-47.049235	96.99205	47.049235
Z58	mag_geo	NaN	47.06277	95.42045	128.167765	-19.353349	17.53117	6	15.552391	5.678506	20.539338	-9.960183	-32.768009	162.478280	34.217680

High-temperature magnetite (geographic) directions for Teel basalt flows

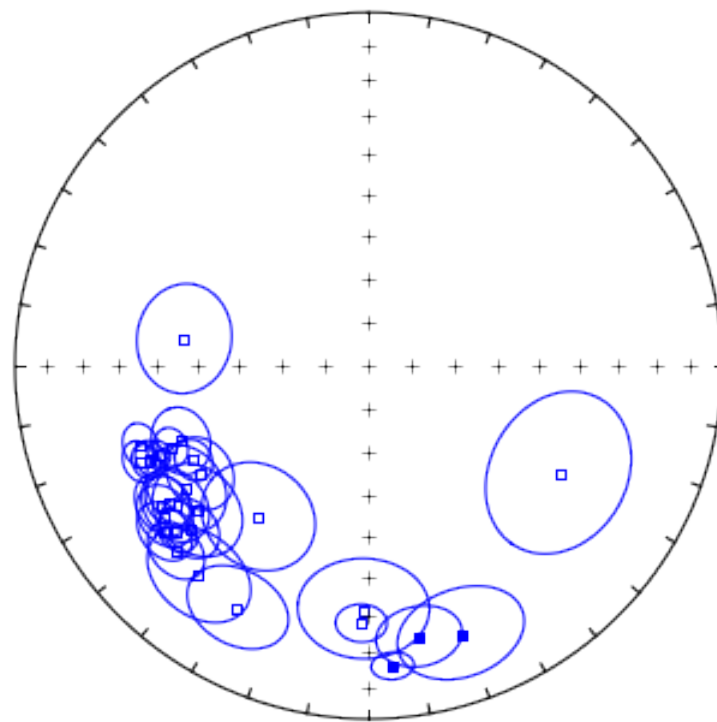


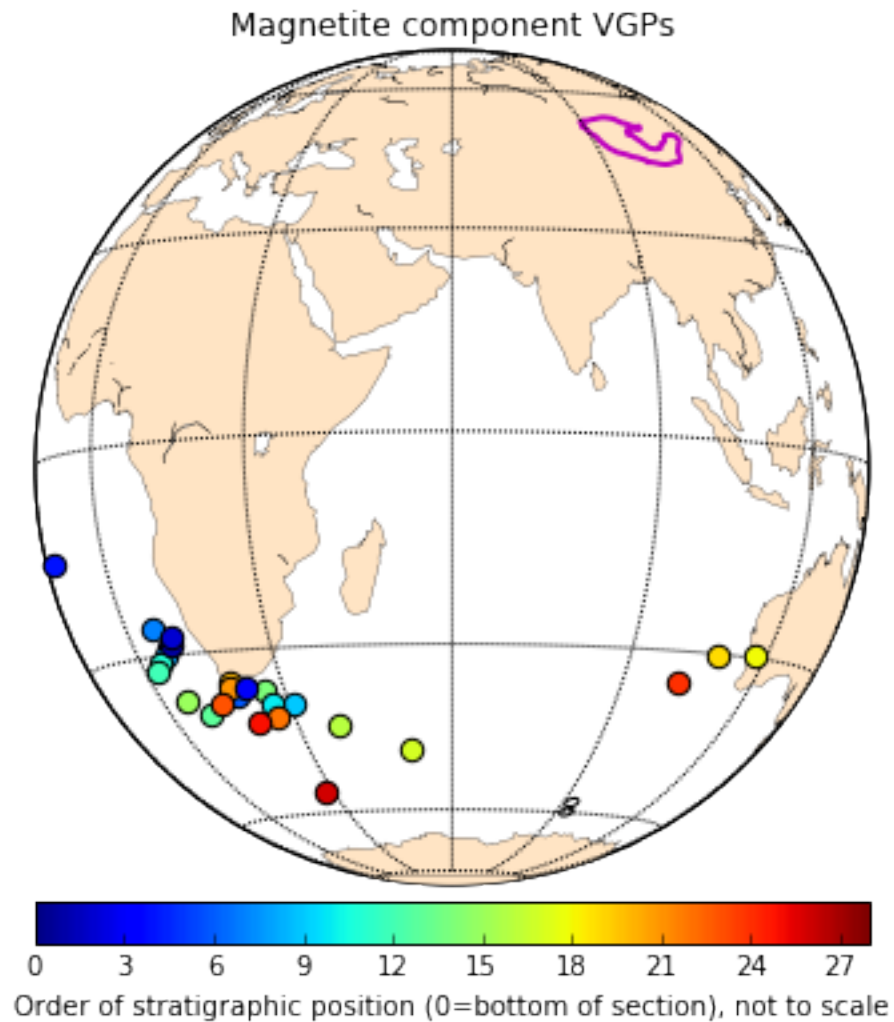


Tilt-corrected coordinates - magnetite [Out\[71\]](#) :

strat_pos	site_lat	site_lon	dec_tc	inc_tc	alpha95	n	k	r	csd	palcolatitude	vgp_lat	vgp_lon	vgp_lat_rev	vgp_lon_rev
Z30_mag	4.0	47.10038	95.37550	278.379367	-46.010280	11.715664	7	27.500012	6.781818	15.446091	-27.381947	-14.408220	340.470733	160.470143
Z31_mag	5.0	47.10049	95.37604	246.928001	-33.319165	3.753646	8	218.734693	7.967798	5.4746791	-18.194560	-28.826591	189.314505	189.314505
Z32_mag	6.0	47.10094	95.37684	234.132395	-32.854953	7.997970	9	42.396758	8.811306	12.439952	-17.895640	-37.203135	19.865666	37.203135
Z33_mag	7.0	47.10107	95.37705	250.685156	-32.176114	4.581718	8	147.127336	7.952422	6.677876	-17.462312	-25.759713	187.086542	187.086542
Z34_mag	8.0	47.10111	95.37712	247.131951	-35.840117	2.844796	10	289.334789	9.968894	4.761948	-19.856873	-29.843343	29.843443	29.843443
Z35_mag	9.0	47.10069	95.37747	226.181747	-25.332749	6.399180	6	110.584559	5.954786	7.702608	-13.316749	-38.856026	31.001433	38.856026
Z36_mag	11.0	47.10221	95.37695	247.531592	-39.317142	4.170654	8	177.361534	7.960533	6.082124	-22.268860	-31.221631	185.451631	185.451631
Z37_mag	12.0	47.10211	95.373971	248.110158	-42.208689	7.223271	9	51.762442	8.845448	11.258425	-24.394791	-32.254972	3.185593	32.254972
Z38_mag	13.0	47.09855	95.38445	237.351592	-42.681665	8.027422	10	37.175977	9.757908	13.284763	-24.753981	-39.808772	190.88772	190.88772
Z39_mag	14.0	47.09860	95.38467	230.880551	-26.400672	6.363220	6	111.827254	5.955288	7.659690	-13.939647	-36.393048	206.087975	206.087975
Z40_mag	15.0	47.09859	95.38474	241.564334	-43.087720	4.522713	9	130.550720	8.938721	7.089170	-25.065058	-37.153357	187.361567	187.361567
Z41_mag	10.0	47.10109	95.37744	229.065098	-29.074319	4.590751	8	146.552710	7.952236	6.690955	-15.536089	-26.422574	206.423205	206.423205
Z42_mag	16.0	47.09577	95.38577	219.102263	-24.487183	11.152830	8	25.6232407	7.726802	16.000239	-12.829071	-42.668510	218.623205	218.623205
Z43_mag	17.0	47.09570	95.38638	208.443581	-22.940527	10.308791	8	29.827403	7.765316	14.831234	-11.948932	-47.500387	231.774438	231.774438
Z44_mag	18.0	47.09571	95.38651	160.933464	20.616106	12.332689	5	39.445745	8.848595	12.896888	-10.652755	-30.988774	297.979721	297.979721
Z45_mag	19.0	47.09562	95.38676	169.431285	22.927525	8.298493	8	45.1511392	7.846192	12.006736	11.9411505	-30.210757	287.371503	287.371503
Z46_mag	20.0	47.09563	95.38692	235.938073	-30.336640	6.7239391	8	68.822329	7.8988289	9.763833	-16.309766	-34.865831	199.681666	199.681666
Z47_mag	21.0	47.09568	95.38727	235.894035	-31.952825	5.439028	8	104.678457	7.933129	7.916922	-17.320745	-35.626283	35.626283	35.626283
Z48_mag	22.0	47.09570	95.38744	237.700040	-32.087392	6.771057	8	67.882078	7.896880	9.831221	-17.406005	-41.018935	206.991501	206.991501
Z49_mag	23.0	47.09581	95.38747	235.973353	-37.612989	9.479951	7	41.489592	6.855420	12.573700	-21.068304	-38.228444	195.348154	195.348154
Z50_mag	24.0	47.09575	95.38781	175.405740	15.829522	3.922362	8	200.402350	7.9656070	5.721812	-8.068715	-34.684493	280.326132	280.326132
Z51_mag	25.0	47.09584	95.38802	229.796663	-36.494284	10.382678	5	55.264038	4.927620	10.895915	-20.299603	-41.77935	201.526132	201.526132
Z52_mag	26.0	47.09583	95.38815	216.149383	-45.789543	12.698064	6	28.791577	5.826338	15.095667	-27.201966	-55.462438	207.657715	207.657715
Z53_mag	1.0	47.09442	95.37205	246.701511	-31.999187	3.599051	8	237.845848	7.970569	5.252151	-17.350100	-28.388510	10.165158	10.165158
Z54_mag	2.0	47.09502	95.37299	247.281883	-30.372895	4.236490	7	203.992983	6.970587	5.671232	-16.332188	-27.276612	10.538894	27.276612
Z55_mag	3.0	47.09525	95.37351	233.513919	-29.023941	6.695472	8	69.401730	7.899138	9.722991	-15.505489	-35.866199	202.430910	202.430910
Z56_mag	NaN	47.06403	95.42075	181.601802	-27.881082	5.069905	6	175.612751	5.971528	6.112233	-14.816796	-57.725144	92.519907	92.519907
Z57_mag	NaN	47.06277	95.42039	181.197564	-31.382585	13.208994	6	26.679224	5.812588	15.681891	-16.961326	-59.882301	273.137125	273.137125
Z58_mag	NaN	47.06277	95.42045	119.444112	-37.602921	17.552705	6	15.519815	5.6777831	-21.061319	-35.140582	20.360882	179.028128	179.028128

High-temperature magnetite (tilt-corrected) directions for Teel basalt flows



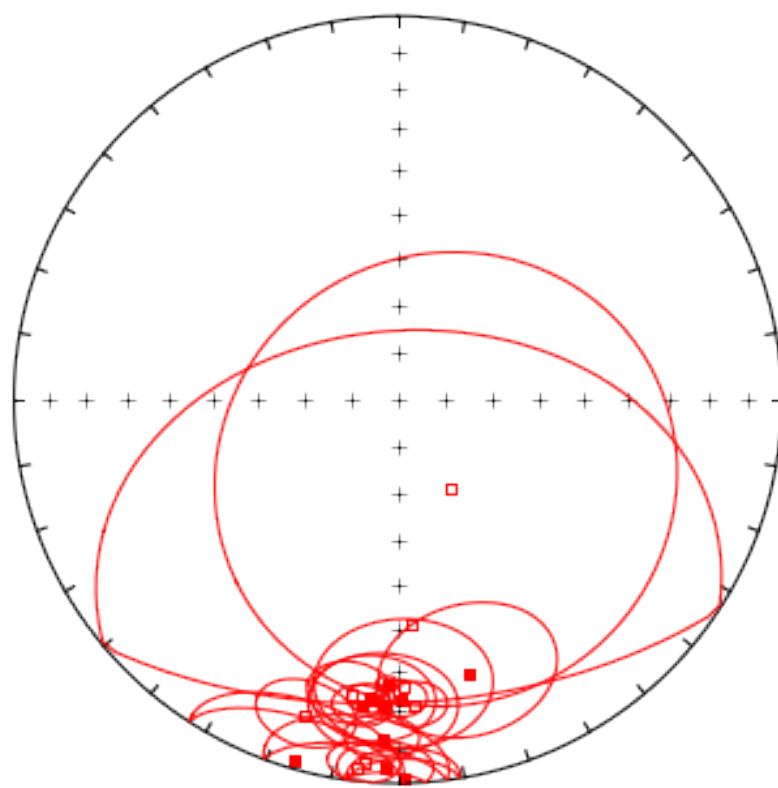


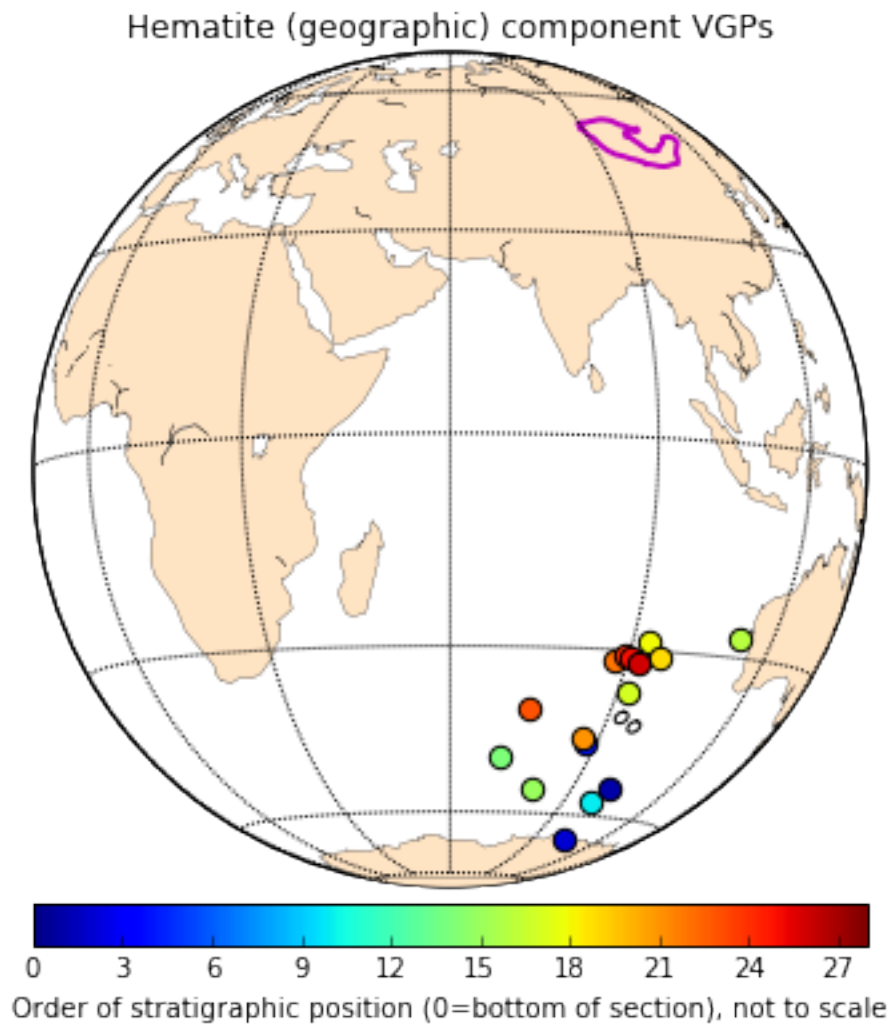
Hematite directions

Geographic coordinates - hematite `Out[74]` :

	strat_pos	site_lat	site_lon	dec_geo	inc_geo	alpha95	n	k	r	csd	paleolatitude	vgp_lat	vgp_lon	vgp_lat_rev	vgp_lon_rev
Z35_hem_geo	4.0	47.10038	95.37550	185.352162	-5.560896	5.747798	6	136.842402	5.963462	6.924281	-2.787011	-45.444034	45.444034	267.7161	
Z30_hem_geo	9.0	47.10069	95.37747	148.79913	-68.20834	49.957167	7	2.413452	4.513935	52.139357	-51.356099	-69.351223	69.351223	135.5221	
Z39_hem_geo	14.0	47.09860	95.38467	196.313095	-15.623428	8.663295	5	78.962990	4.949343	9.115347	-7.956659	-48.458523	48.458523	255.6722	
Z40_hem_geo	15.0	47.09859	95.38474	189.173133	-23.507115	7.794855	7	60.926778	6.901521	10.377217	-12.269627	-54.326542	54.326542	255.6722	
Z41_hem_geo	10.0	47.10109	95.37744	178.834097	-26.223550	16.086290	5	23.576274	4.830338	16.681974	-13.836835	56.721476	56.721476	271.1334	
Z42_hem_geo	16.0	47.09577	95.38577	165.448451	27.28167	16.388007	6	17.664613	5.716948	19.272274	14.457588	-27.077402	11.1243174	292.174	
Z43_hem_geo	17.0	47.09570	95.38638	182.753379	12.734651	6.220142	8	80.262873	7.912787	9.041233	6.446942	-36.401745	36.401745	270.0451	
Z44_hem_geo	18.0	47.09571	95.38651	182.138446	26.690156	2.023836	7	890.663468	6.993263	14.169891	-28.764330	93.02083	28.764330	272.0333	
Z45_hem_geo	19.0	47.09562	95.38676	179.431606	23.111384	4.657126	8	142.431974	7.950854	12.045434	-30.856760	96.034300	30.856760	272.0333	
Z46_hem_geo	21.0	47.09568	95.38727	186.530284	-3.818259	18.506577	7	14.407211	6.675791	18.828771	-44.460110	86.223719	44.460110	266.377	
Z47_hem_geo	22.0	47.09570	95.38744	186.680865	20.745840	5.248580	8	112.342494	7.937691	10.724316	-31.873027	26.073812	31.873027	266.377	
Z48_hem_geo	23.0	47.09581	95.38747	196.040735	2.334680	17.030887	7	13.514021	6.556017	22.033969	1.167825	-39.732489	74.334390	39.732489	
Z49_hem_geo	24.0	47.09575	95.38781	185.576609	22.848691	3.695319	8	225.663876	7.968980	11.897134	-30.796567	89.031882	30.796567	266.377	
Z50_hem_geo	25.0	47.09584	95.38802	184.630448	22.563173	10.926624	5	49.990867	4.919985	11.456176	11.736415	-31.022182	31.022182	277.5201	
Z51_hem_geo	26.0	47.09583	95.38815	182.775348	21.100104	13.120981	6	27.028581	5.814990	15.581078	10.920183	-31.930956	31.930956	277.5201	
Z52_hem_geo	1.0	47.09442	95.37205	176.883446	-21.454440	5.750351	7	111.157505	6.946023	7.652731	-11.116766	-53.926099	53.926099	282.111	
Z53_hem_geo	2.0	47.09502	95.37299	176.563071	-41.301285	63.346282	7	1.863743	3.780672	59.332417	-66.458593	103.271614	66.458593	282.111	
Z54_hem_geo	NaN	47.06403	95.42075	179.194265	1.511589	8.593573	6	61.741195	5.919017	10.308548	0.755926	-42.174837	96.507901	42.174837	
Z55_hem_geo	NaN	47.06277	95.42039	181.947532	4.332196	7.473594	4	152.109621	3.980277	6.567600	2.169198	-40.738280	92.851012	272.803	

Hematite directions from Teel basalt flows in geographic coordinates

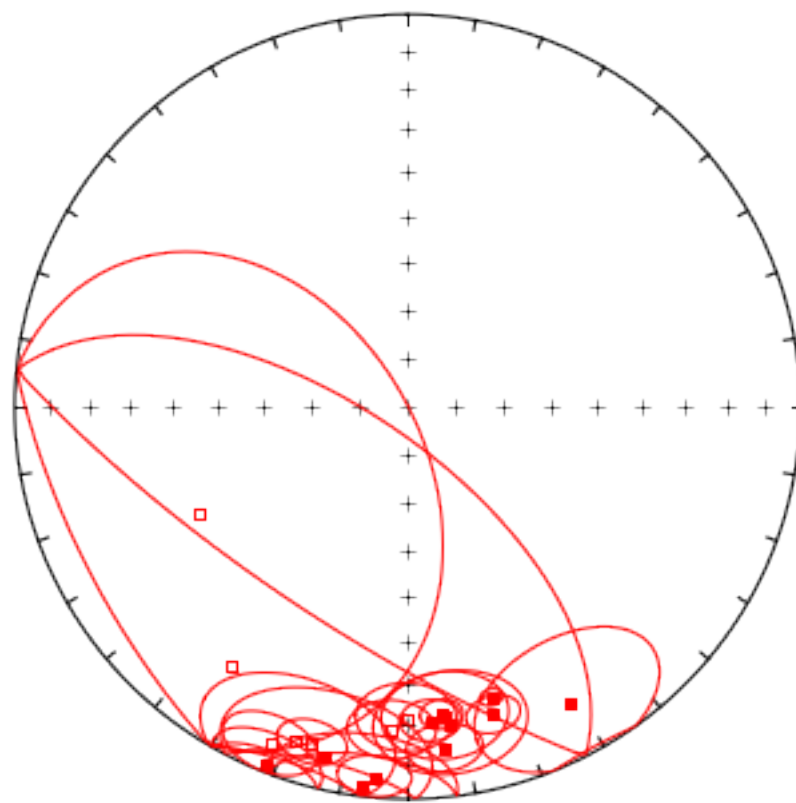


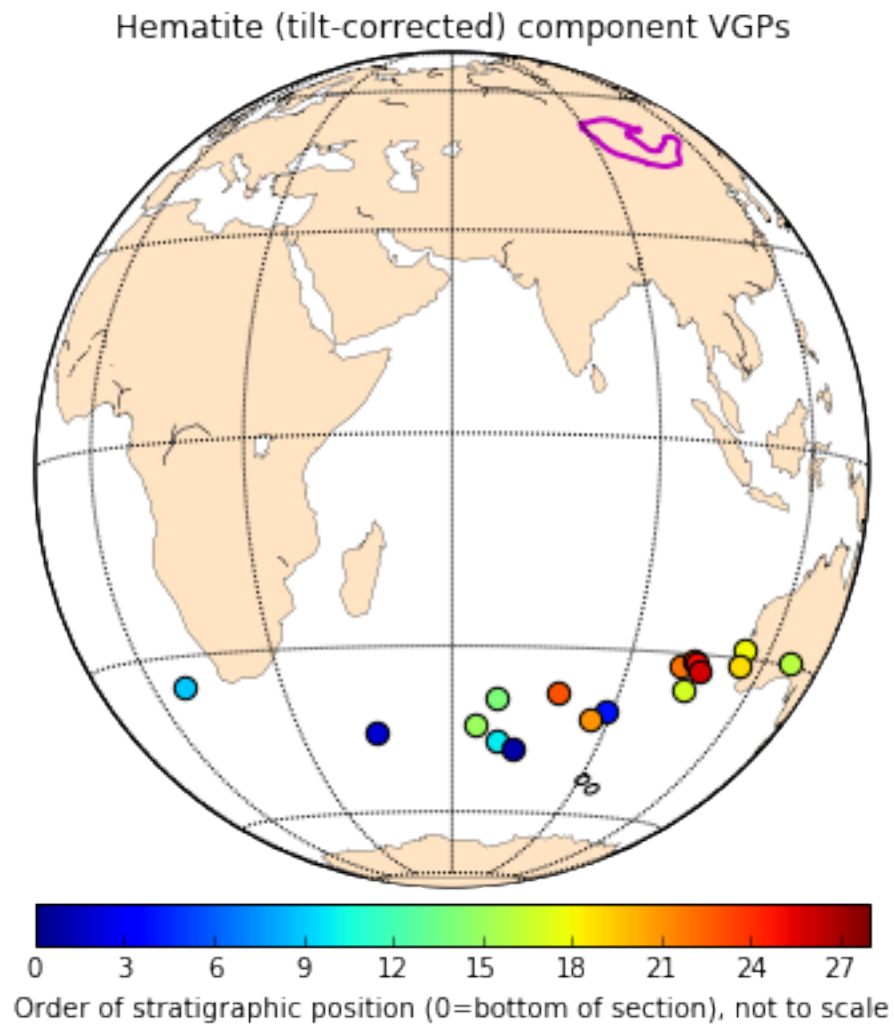


Tilt-corrected coordinates - hematite [Out \[77\]](#) :

strat_pos	site_lat	site_lon	dec_tc	inc_tc	alpha95	n	k	r	csd	paleolatitude	vgp_lat	vgp_lon	vgp_lat_rev	vgp_lon_rev
Z35_hem	4.0	47.10038	95.37550	185.11431	6.025809	5.727598	6	137.802632	5.963716	6.900114	3.021259	-39.676603	88.733786	39.6776603
Z30_hem	9.0	47.10069	95.37747	242.928054	-40.237690	49.931876	7	2.414928	4.515454	52.123423	-22.933069	-34.802858	188.295178	34.802858
Z39_hem	14.0	47.09860	95.38467	201.539571	2.413034	8.658960	5	79.041121	4.949393	9.110841	1.207052	-38.143076	247.563030	38.143076
Z40_hem	15.0	47.09859	95.38474	202.157748	-7.928196	7.788149	7	61.030111	6.901688	10.388429	-42.830083	64.518459	42.830083	64.518459
Z41_hem	10.0	47.10109	95.38774	198.411151	-11.058439	16.113432	5	23.500114	4.829788	16.708984	-45.565273	68.6368517	45.565273	248.6368517
Z42_hem	16.0	47.09577	95.38577	151.386122	14.995751	16.374487	6	17.692229	5.717390	19.257227	7.628503	-29.676516	128.501026	29.676516
Z43_hem	17.0	47.09570	95.38638	173.787706	13.587096	6.227989	8	80.063147	7.912569	9.032503	6.890414	-35.733259	102.991555	35.733259
Z44_hem	18.0	47.09571	95.38651	163.946455	23.981346	2.033549	7	882.18419	6.938199	2.727126	12.539568	113.302682	28.638505	113.302682
Z45_hem	19.0	47.09562	95.38676	164.416633	19.683336	4.665334	8	141.934618	7.950682	6.798934	10.144077	-31.097230	293.374720	31.097230
Z47_hem	21.0	47.09568	95.38727	186.913270	14.418197	2.679432	7	18.418197	6.675322	18.842390	1.340449	-41.186055	266.186460	41.186055
Z48_hem	22.0	47.09570	95.38744	175.819816	20.880528	5.256939	8	111.988554	7.937494	7.654172	10.798704	-31.985346	280.230686	31.985346
Z49_hem	23.0	47.09581	95.38747	193.267745	9.061857	17.012716	7	13.540873	6.556897	22.012111	4.559441	-37.033236	258.733211	37.033236
Z50_hem	24.0	47.09575	95.38781	173.713227	22.176830	3.699165	8	225.196841	7.968916	5.397639	78.733953	102.587676	282.587676	102.587676
Z51_hem	25.0	47.09584	95.38802	173.080330	21.475208	10.923983	5	50.015473	4.929025	11.453358	-31.115698	31.115698	31.115698	31.115698
Z52_hem	26.0	47.09583	95.38815	172.236460	19.385124	13.100041	6	27.108018	5.815560	15.557081	11.129977	-31.144685	283.352735	31.144685
Z53_hem	1.0	47.09442	95.37205	195.874742	-12.092261	5.754882	7	110.984038	6.945938	7.638733	32.507612	104.465028	32.507612	284.465028
Z54_hem	2.0	47.09502	95.37299	214.227658	-21.424836	63.339718	7	1.863930	3.750994	59.329441	6.114213	71.795927	251.955227	46.812655
Z56_hem	NaN	47.06403	95.42075	180.301491	-21.711722	8.592210	6	61.760484	5.919042	10.36938	-11.100316	43.897588	45.377588	225.377588
Z57_hem	NaN	47.06277	95.42039	182.841002	-18.592084	7.462069	4	152.576865	3.980338	6.557536	-9.547317	-52.406934	270.824846	52.406934

Hematite (tilt-corrected) directions from Teel basalt flows

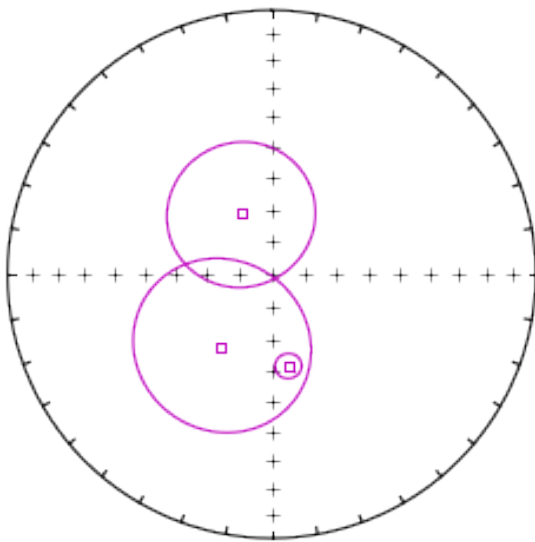




Mid-temperature directions Out[80]:

	strat_pos	site_lat	site_lon	dec_geo	inc_geo	alpha95	n	k	r	csd	paleolatitude	vgp_lat	vgp_lon	vgp_lat_rev	vgp_lon_rev
Z42_mid	16.0	47.09577	95.38577	332.936127	-68.973663	22.704625	4	17.342624	3.827016	19.440359	-52.447527	-12.194273	12.194273	111.86715	111.86715
Z43_mid	17.0	47.09570	95.38638	214.749151	-62.316153	27.256978	4	12.329873	3.756688	23.067776	-43.621783	-65.542782	0.679322	180.679322	180.679322
Z58_mid	NaN	47.06277	95.42045	169.642703	-61.042884	3.980349	6	284.324122	5.982414	4.803725	-42.101543	-81.121562	155.222442	81.121562	335.222442

Mid-temperature directions from Teel basalt flows in geographic coordinates



Flow Z58 yielded a completely different mid-temperature result compared to all other sites. The magnetite direction is completely different than all other results. The mean direction is very imprecise (SE and moderately-shallow down) but is closest in orientation to the Middle to Late Carboniferous ‘A’ component of Edel et al. (2014).

2.5 Paleomagnetic Poles for the Teel Formation

We interpret the primary paleomagnetic direction for the Teel basalts to be held by (titanio)magnetite with a secondary remanence held by hematite holding a distinct direction. However, demagnetization data from some sites within the most oxidized flows show similarities between the remanence directions of magnetite and hematite that correspond to the hematite direction seen in other flows that have a distinct magnetite direction. We suspect that these flows were overprinted in the remagnetization event that led to the hematite overprint. As a result we exclude this flows where magnetite corresponds to the distinct hematite direction from the calculation of the mean magnetite pole.

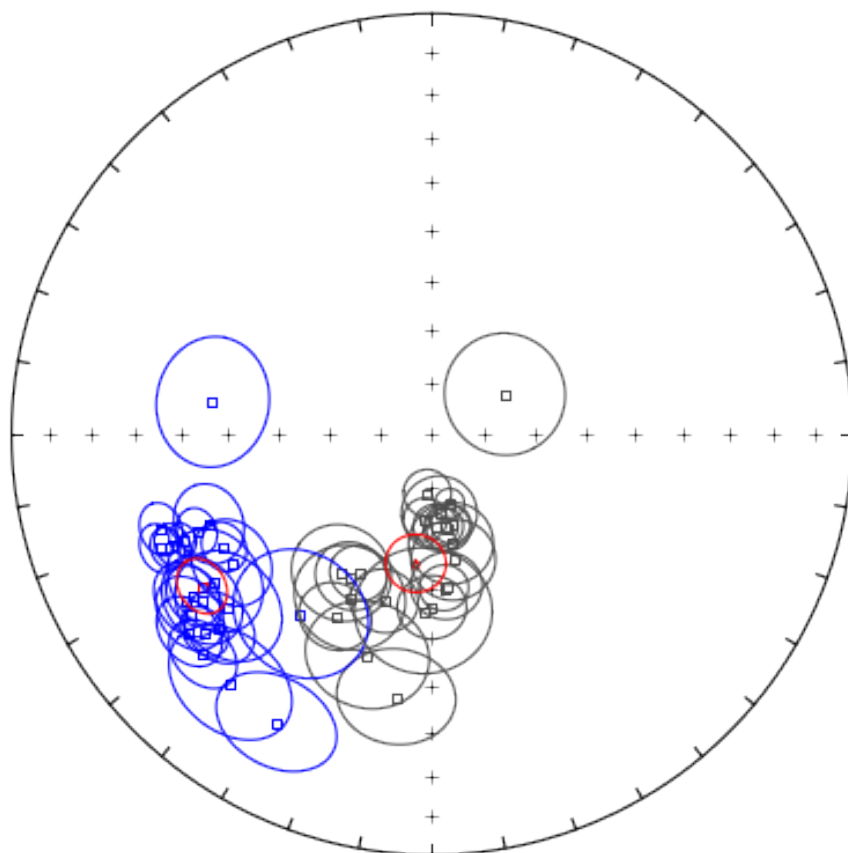
Primary magnetite pole - including tilt test

```
Out[84]: {'alpha95': 5.016359320556993,
 'csd': 13.24736661179077,
 'dec': 236.55328337929615,
 'inc': -34.725447678823137,
 'k': 37.386165760749734,
```

```
'n': 23,  
'r': 22.411547037457986}
```

```
Out[85]: {'alpha95': 5.7013669696125859,  
'csd': 14.999123289480917,  
'dec': 187.16163375289389,  
'inc': -64.697686409549988,  
'k': 29.163408949361457,  
'n': 23,  
'r': 22.245630027744692}
```

High-temperature magnetite (geographic: gray, tilt-corrected: blue) directions



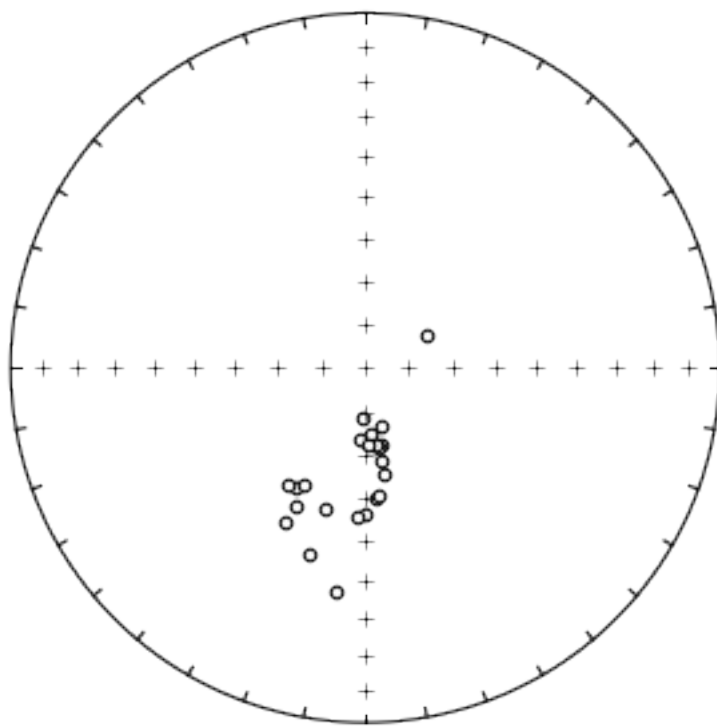
Bootstrap fold (tilt) test (Tauxe and Watson, 1994)

We quote bootstrap tilt test values for two different confidence intervals: 99% and 95%. Because the bootstrap pseudo-populations are randomly chosen, values for the confidence intervals will likely

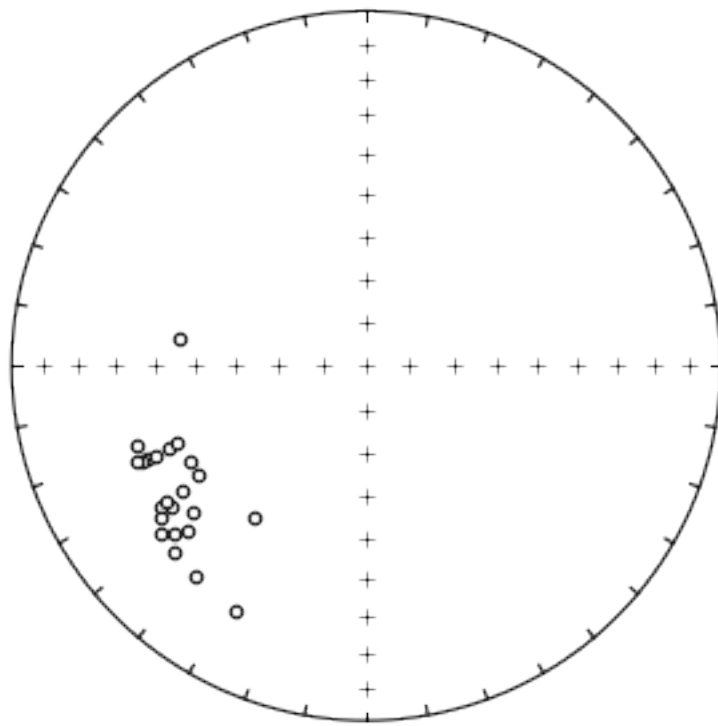
be different from those quoted in the text; results will change slightly each time the bootstrap test is run.

doing 1000 iterations...please be patient...

Geographic

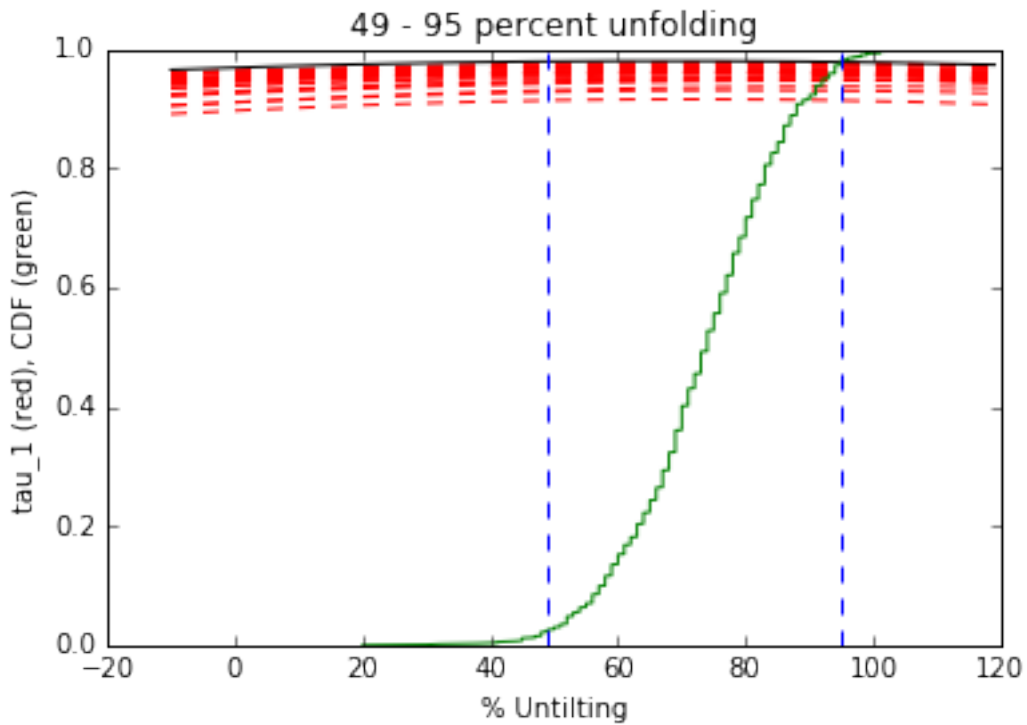


Tilt-corrected



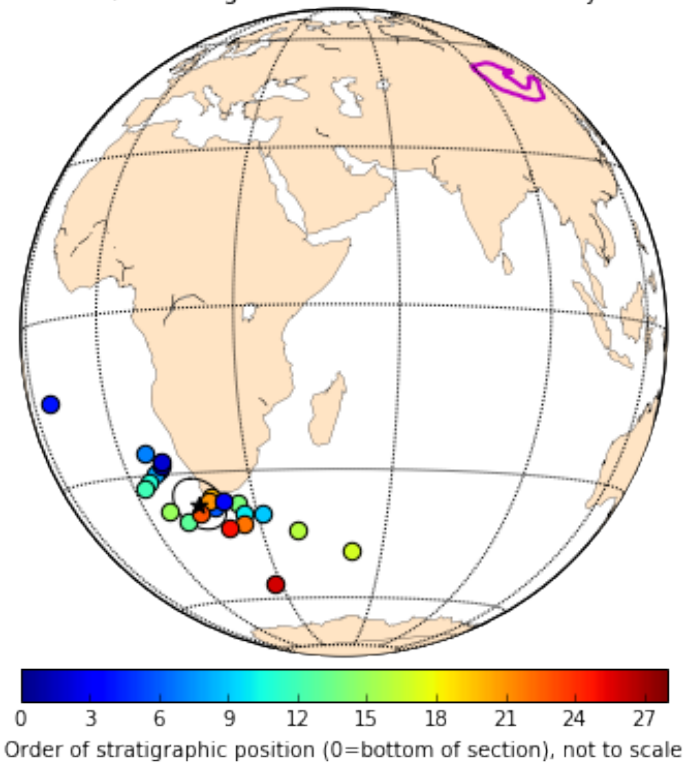
tightest grouping of vectors obtained at (99% confidence bounds):
41 - 101 percent unfolding

tightest grouping of vectors obtained at (95% confidence bounds):
49 - 95 percent unfolding
range of all bootstrap samples:
20 - 104 percent unfolding



Below the tilt-corrected magnetite VGPs are plotted on the globe and shaded according to their relative stratigraphic positions.

Primary magnetite VGPs (excluding those identical to secondary hematite components)

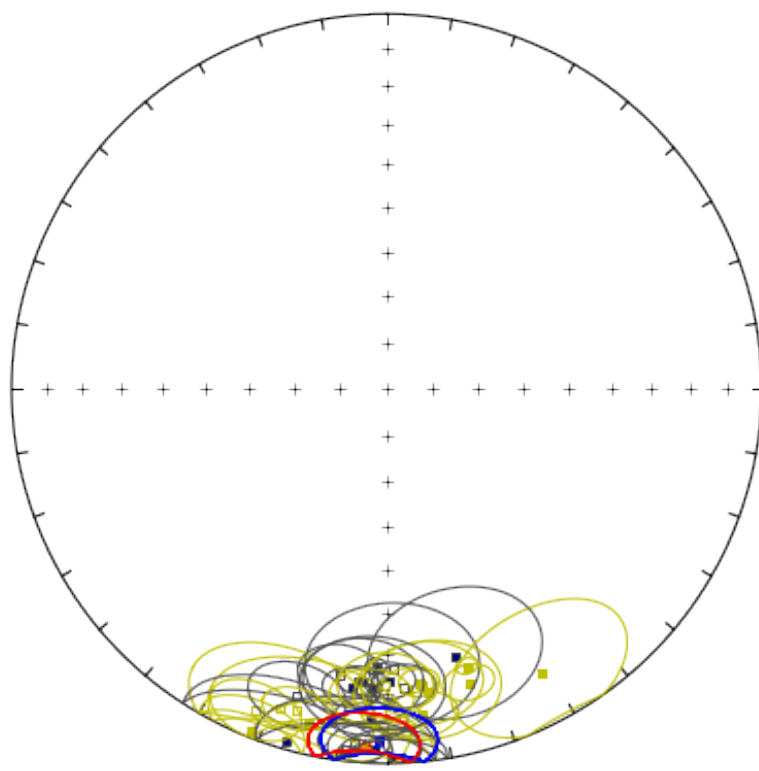


Secondary hematite pole - including tilt test

```
Out[91]: {'alpha95': 8.9877257442158918,
          'csd': 19.806244991238223,
          'dec': 183.64700144578103,
          'inc': 5.4005776522632472,
          'k': 16.724985285223418,
          'n': 17,
          'r': 16.043347439346565}
```

```
Out[92]: {'alpha95': 9.4366310429368436,
          'csd': 20.733802634569454,
          'dec': 181.16680682161584,
          'inc': 6.4513316241785841,
          'k': 15.262023482436897,
          'n': 17,
          'r': 15.95164622054131}
```

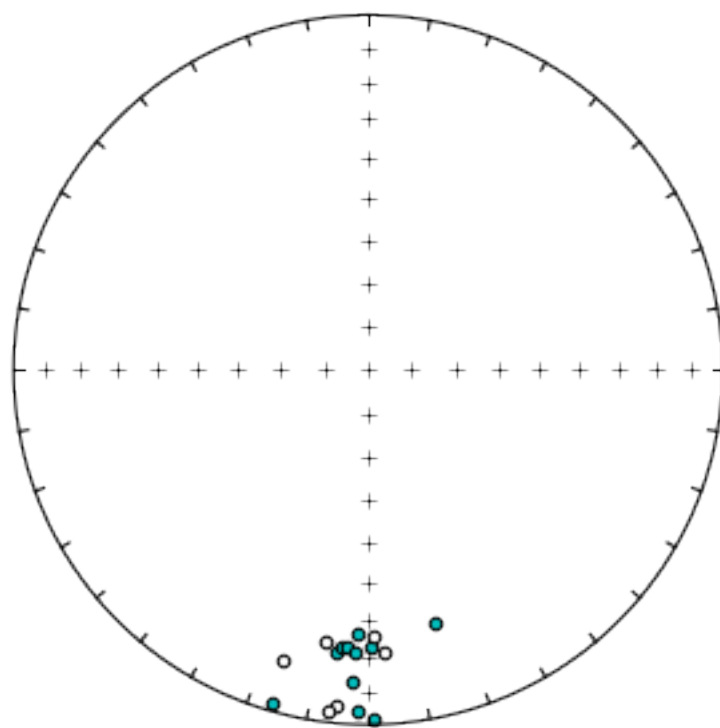
High-temperature hematite (geographic: gray/red, tilt-corrected: yellow/blue) directions



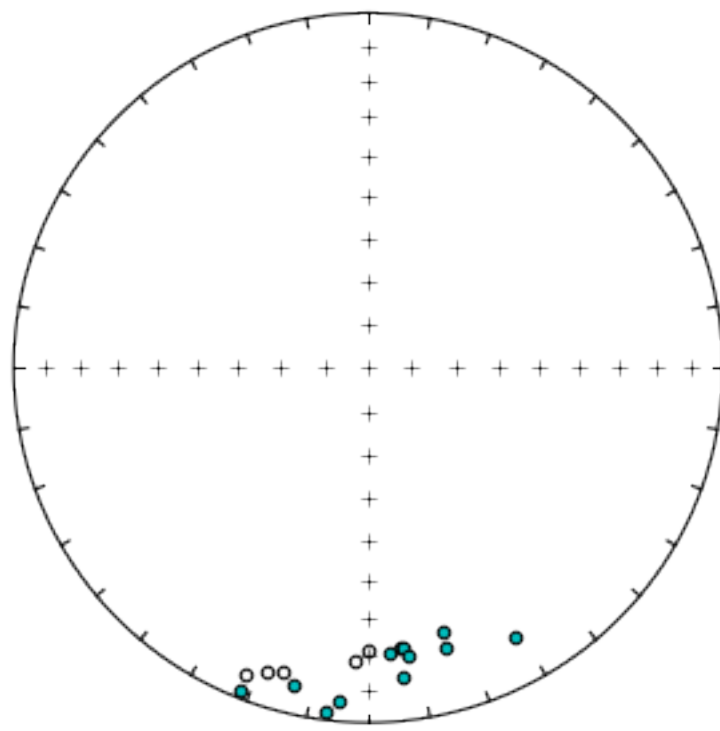
Bootstrap fold test (Tauxe and Watson, 1994)

doing 1000 iterations...please be patient...

Geographic



Tilt-corrected

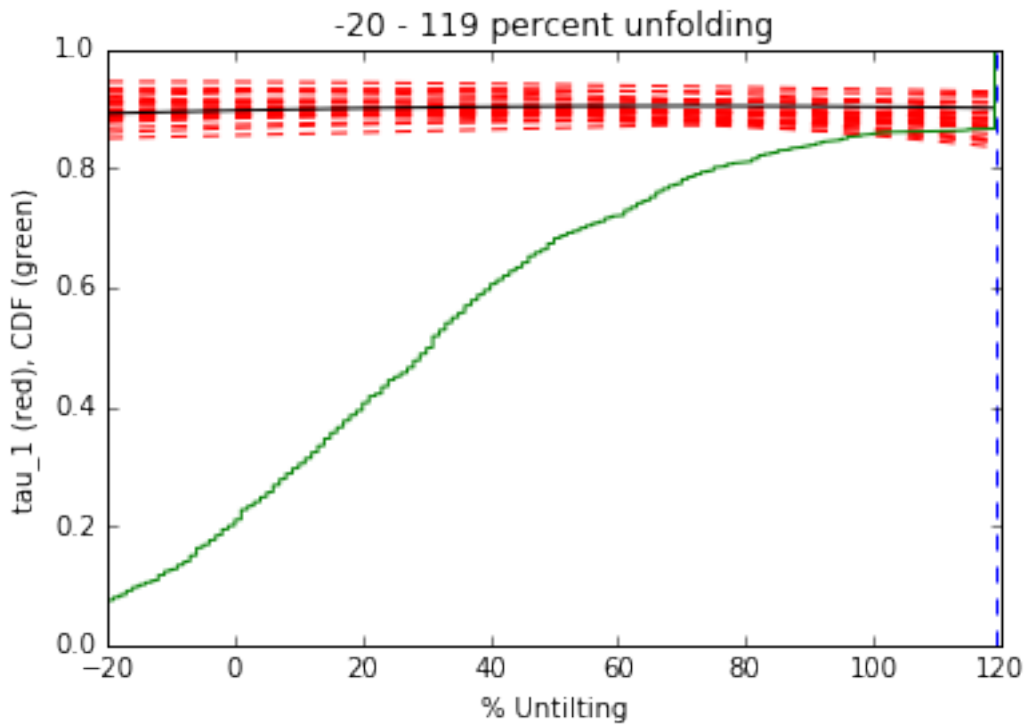


tightest grouping of vectors obtained at (95% confidence bounds):

-20 - 119 percent unfolding

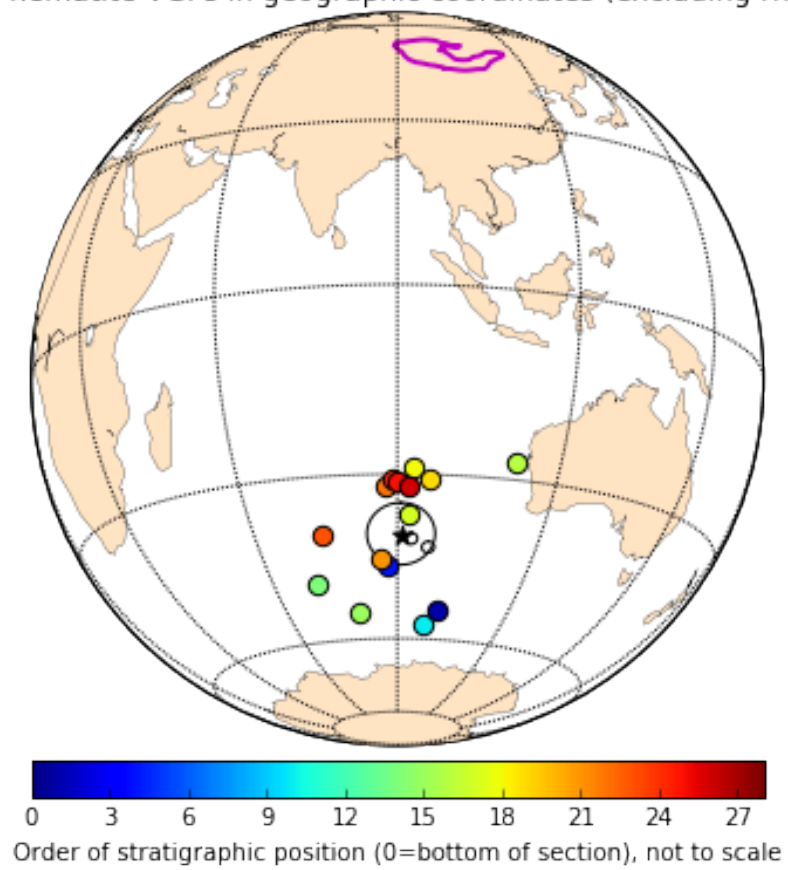
range of all bootstrap samples:

-20 - 119 percent unfolding

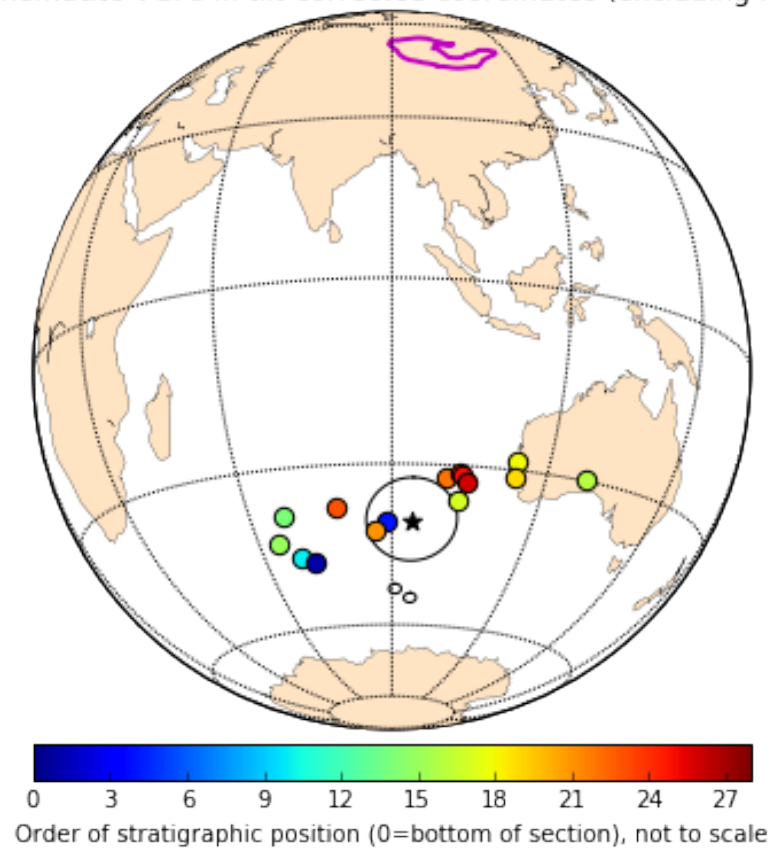


Below the geographic and tilt-corrected hematite VGPs are plotted on the globe and shaded according to their relative stratigraphic positions. Note the similar positions between the two coordinate system means.

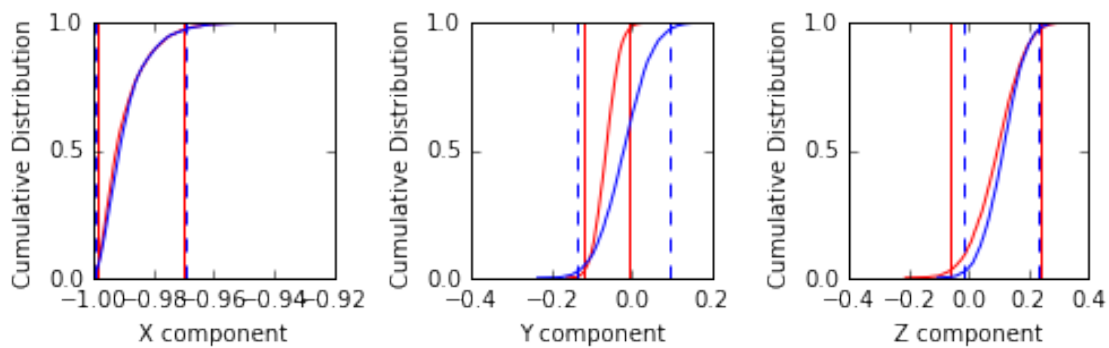
Secondary hematite VGPs in geographic coordinates (excluding rhyolite Z30)



Secondary hematite VGPs in tilt-corrected coordinates (excluding rhyolite Z30)



Common mean test (bootstrap method)



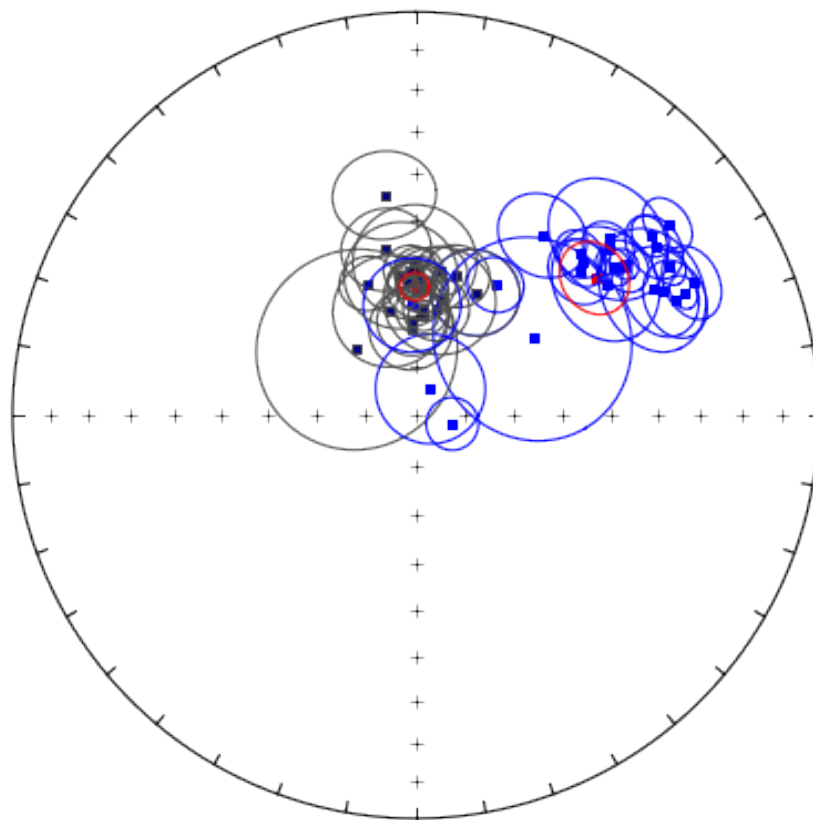
The above test confirms that the geographic and tilt corrected hematite mean directions are statistically indistinguishable and share a common mean.

Present local field overprint - negative fold test **Out[98]:**

Out[99]:

A number of poles are excluded because of inconsistencies between samples within site which resulted in large a95 values for these sites: Z45, Z51, and Z52.

Low-temperature magnetization (geographic: gray, tilt-corrected: blue) directions

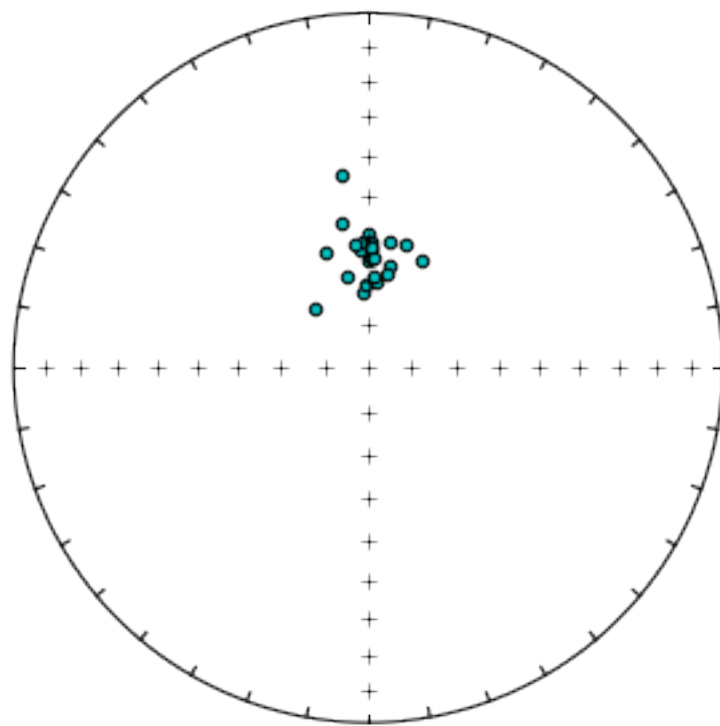


Bootstrap fold test (Tauxe and Watson, 1994)

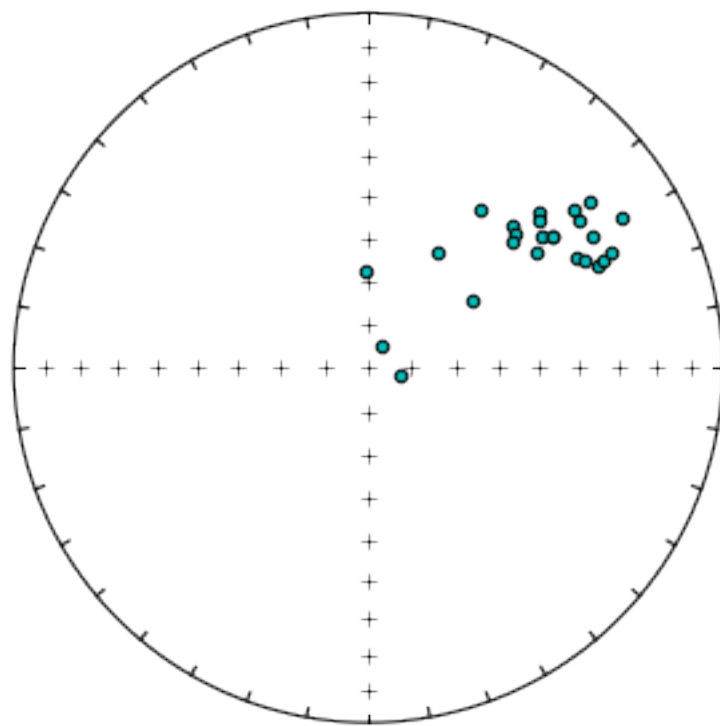
doing 1000 iterations...please be patient...

strat_pos	site_lat	site_lon	dec_tc	inc_tc	alpha95	n	k	r	cstd	paleolatitude	vgp_lat	vgp_lon	vgp_rev	vgp_lat_rev	vgp_lon_rev
Z30_low	4.0	47.10038	95.37550	62.140855	33.713657	11.463681	7	28.680029	6.790795	15.124995	18.450285	32.248029	192.800152	-32.248029	
Z31_low	5.0	47.10049	95.37604	59.403835	27.8676060	3.615270	8	235.275142	7.970304	7.970324	14.813793	31.483337	18.002746	18.002746	
Z32_low	6.0	47.10094	95.37684	25.802094	62.301378	8.844441	8	40.180191	7.857585	12.775475	43.63851	186.500445	71.621088	6.85018088	
Z33_low	7.0	47.10107	95.37705	54.8002714	28.343404	6.0096620	8	85.916769	7.918526	8.73684	15.094685	34.7202681	201.658195	-34.7202681	
Z34_low	8.0	47.10111	95.37712	52.668703	27.653908	3.866823	10	157.041051	9.942690	6.463659	14.681124	35.784873	203.849471	-35.784873	

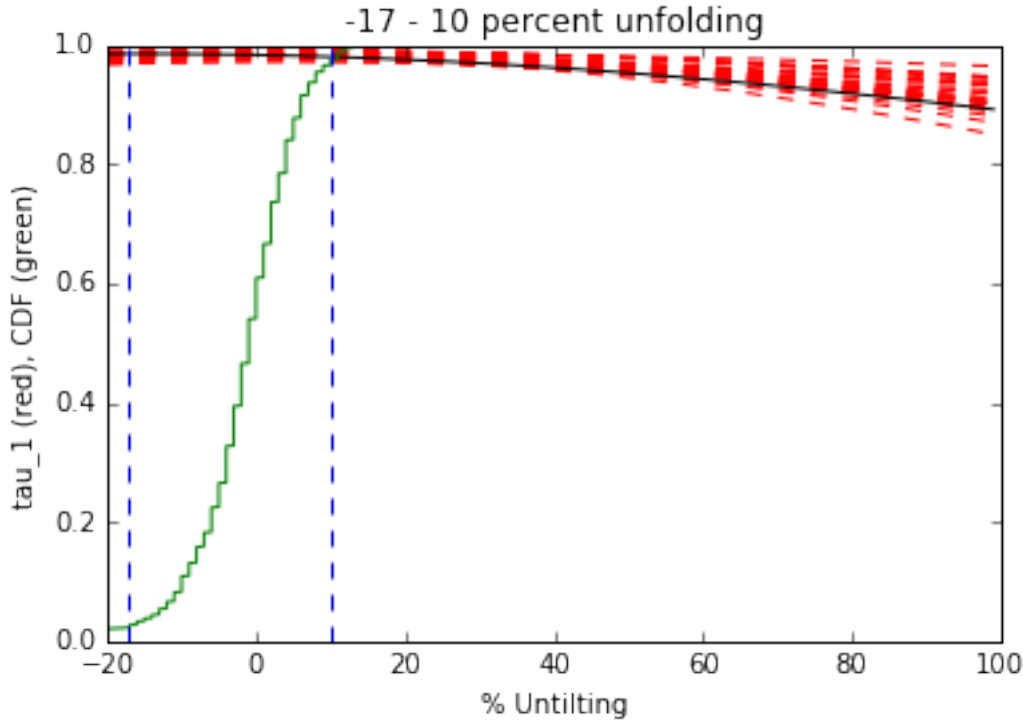
Geographic



Tilt-corrected



tightest grouping of vectors obtained at (95% confidence bounds):
-17 - 10 percent unfolding
range of all bootstrap samples:
-20 - 21 percent unfolding



Teel poles summary `Out[103]`:

	Pole_Lat	Pole_Long	A_95	K	CSD	N	r	Paleolat
Teel_magnetite_tc	-36.417598	16.244116	5.306437	33.514632	13.991613	23	22.343570	-19.113506
Teel_magnetite_geo	-85.857354	342.309952	8.111758	14.902542	20.982384	23	21.523742	-46.604795
Teel_hematite_tc	-39.599546	94.136871	7.315512	24.749088	16.281912	17	16.353512	3.235922
Teel_hematite_geo	-40.034308	90.750359	5.353746	45.365533	12.026022	17	16.647309	2.706300

3 Pole compilation for Siberia, North China, and Mongolian terranes

3.1 Import existing paleomagnetic data

3.1.1 Siberia

Note that a rotation needs to be applied for relative rotation between Aldan and Anabar blocks before the Devonian Period due to Devonian rifting in the Viljuy Basin near the centre of the craton. Here are two rotations used in the literature: Euler Pole (Lat, Long, rotation)

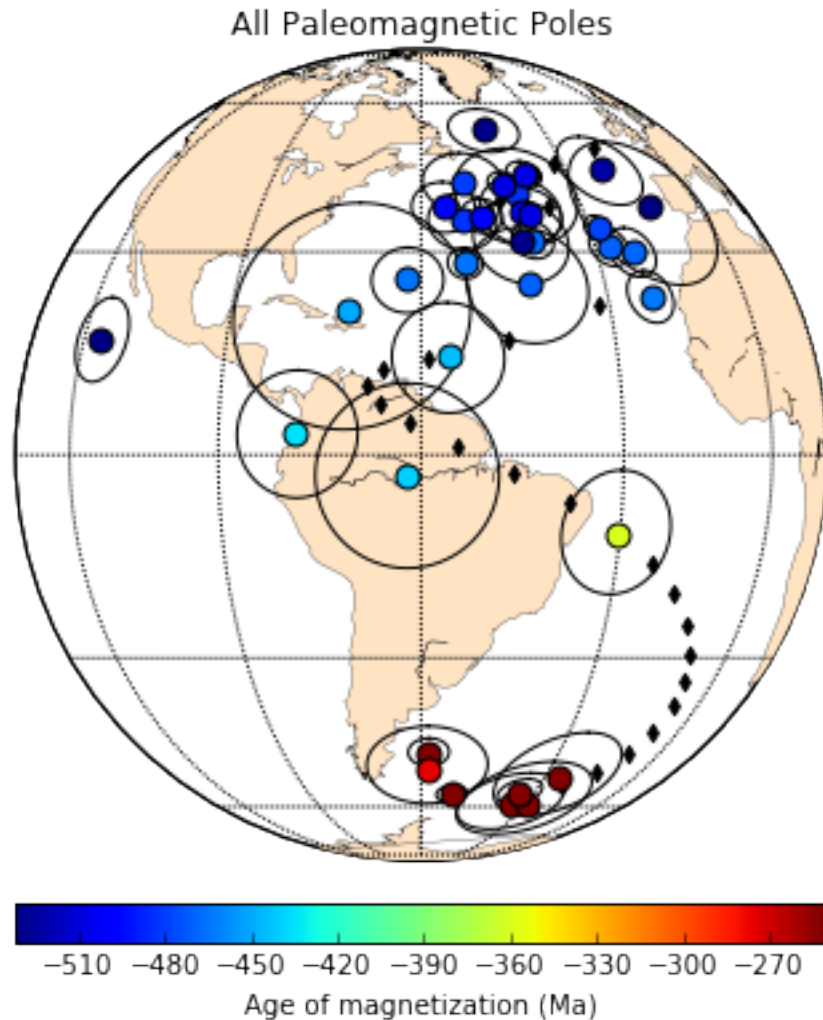
- (60°N , 120°E , 13°) from Smethurst et al. (1998)
- (60°N , 115°E , 25°) everything pre-Devonian (Evans, 2009)
- (60°N , 120°E , 16°) Cambrian to Early Silurian correction (Cocks and Torsvik, 2007)

- (62°N, 117°E, 20°) pre-Devonian (Pavlov et al. (2008) also used in Powerman et al. (2013))

Most Siberia poles are imported from Cocks and Torsvik (2007) in which the data are rotated from the “southern” Siberia (Aldan) into the northern Siberia (Anabar) reference frame according to Smethurst et al. (1998), which the authors argue brings N and S pre-Devonian poles into the best agreement.

Torsvik et al. (2012) updated their Siberia apparent polar wander path by adding data from Shatsillo et al. (2007) that superceded results from the coeval Lena River sediments (Rodianov et al., 1982; Torsvik et al., 1995). However, there are more results from Siberia that must have been discarded by Cocks and Torsvik (2007) and subsequently by other authors. We discuss these poles later on.

Below we plot the paleomagnetic data compiled by Cocks and Torsvik (2007) for Siberia, shaded according to age.



In the following analyses, we update this pole list to include additional poles from the area in order to construct a paleolatitdue plot of Siberia through the Phanerozoic Eon.

We use the Haversine formula to calculate the distance between the VGPs and a reference point on a given plate. This is then used to calculate the paleolatite of the reference point.

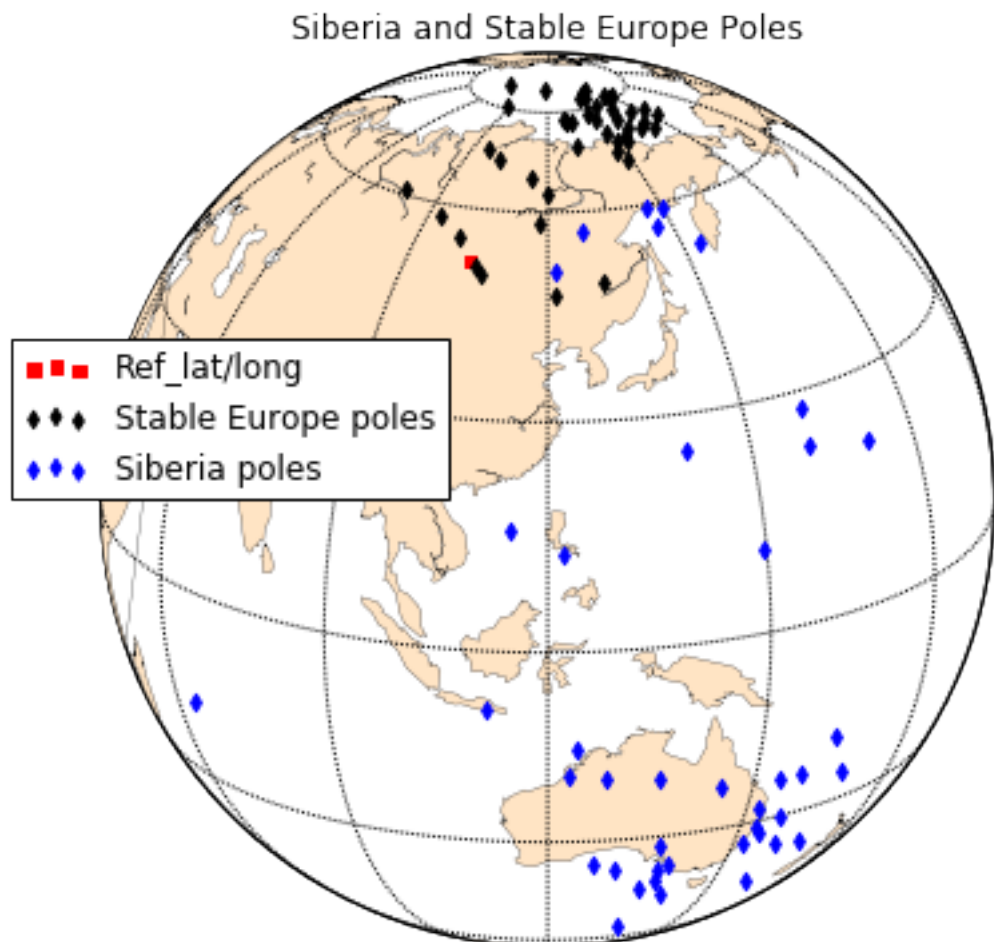
We first load poles for stable Europe from 250 Ma to the present day from Torsvik et al. (2012).

Out [108] :

	high_age	low_age	median_age	A95	PLat	PLon	Paleolat	PLat_N	PLon_N
0	1.0	0.0	0.5	3.6	-80.6	267.5	60.64	80.6	87.5
1	1.0	0.0	0.5	4.4	-86.4	296.1	55.21	86.4	116.1
2	10.0	6.0	8.0	12.9	-84.3	357.7	52.91	84.3	177.7
3	11.0	8.0	9.5	1.8	-78.9	328.3	58.73	78.9	148.3
4	11.0	9.0	10.0	3.5	-77.4	314.2	61.90	77.4	134.2

Poles from Siberia are then loaded (545 to 250 Ma). Most of the poles were taken from Cocks and Torsvik (2007) and Torsvik et al. (2012), but we also added additional data gathered from the Global Paleomagnetic Database.

Out [109] :



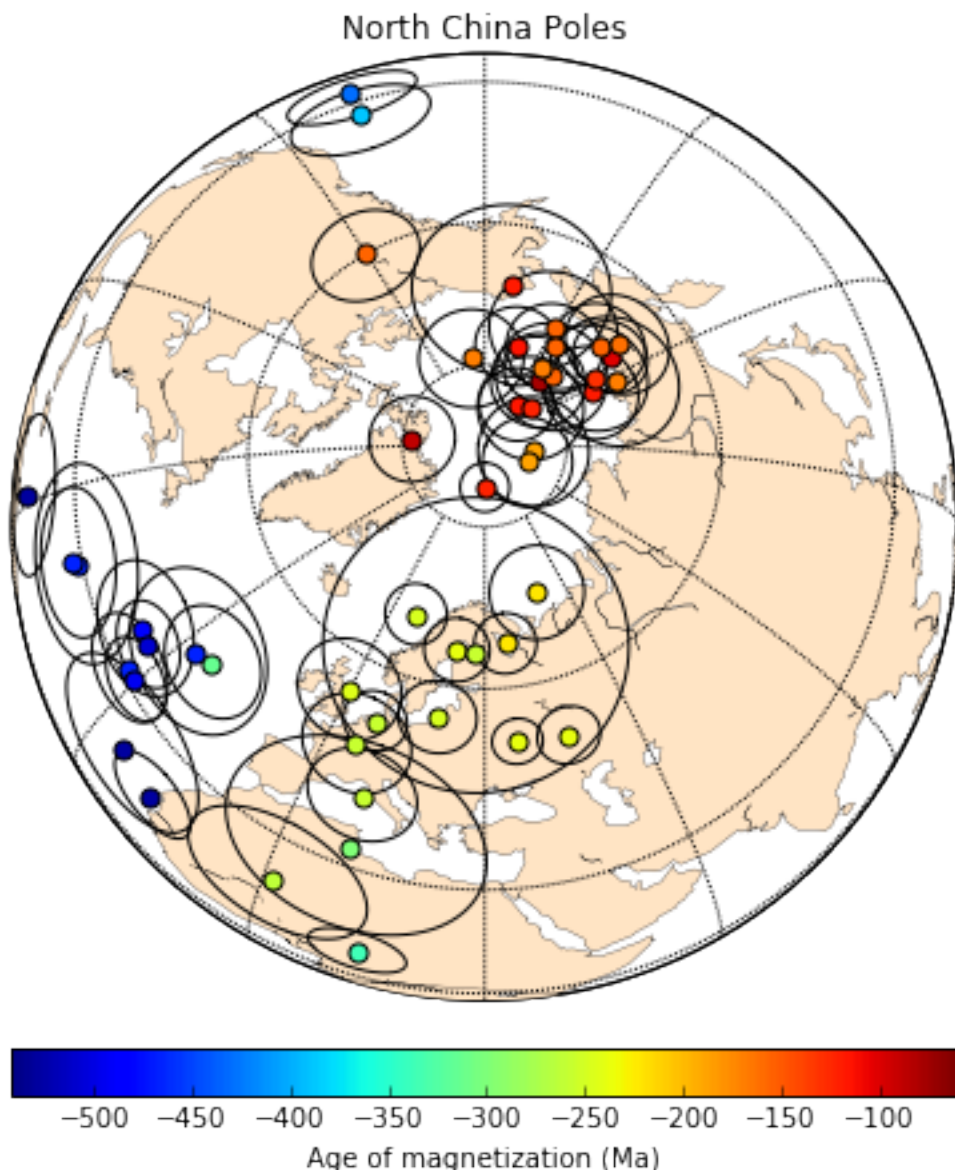
	plate_ID	high_age	low_age	median_age	A95	PLat	FLon	Reference	Paleolat	PLat_N	PLon_N
0	401	245	243	244.0	10.0	-59.0	330.0	GPDB2832, Gurevitch et al. (1995) from Cocks a... Walderhaug et al. (2005) from Cocks and Torsvik... Gurevitch et al. (2004) from Cocks and Torsvik... GPDB3486, Kravchinsky et al. (2002) from Cocks... Pavlov and Gallet (1996) from Cocks and Torsvik... Pisarevsky et al. (2006) from Cocks and Torsvik... GPDB1991, Davydov and Kravchinsky (1973)	63.18 65.34 65.00 59.48 74.99 56.6 50.5	59.0 59.3 56.2 52.8 56.6 56.6 50.5	150.0 145.8 146.0 154.4 127.9 121.4 170.0
1	401	255	238	248.0	7.8	-59.3	325.8	Walderhaug et al. (2005) from Cocks and Torsvik... Gurevitch et al. (2004) from Cocks and Torsvik... GPDB3486, Kravchinsky et al. (2002) from Cocks... Pavlov and Gallet (1996) from Cocks and Torsvik... Pisarevsky et al. (2006) from Cocks and Torsvik... GPDB1991, Davydov and Kravchinsky (1973)	65.34 65.00 59.48 74.99 56.6 50.5	59.3 56.2 52.8 56.6 56.6 50.5	145.8 146.0 154.4 127.9 121.4 170.0
2	401	253	248	251.0	3.3	-56.2	326.0	Walderhaug et al. (2005) from Cocks and Torsvik... Gurevitch et al. (2004) from Cocks and Torsvik... GPDB3486, Kravchinsky et al. (2002) from Cocks... Pavlov and Gallet (1996) from Cocks and Torsvik... Pisarevsky et al. (2006) from Cocks and Torsvik... GPDB1991, Davydov and Kravchinsky (1973)	65.00 59.48 74.99 56.6 56.6 50.5	56.2 52.8 56.6 56.6 56.6 50.5	146.0 154.4 127.9 121.4 121.4 170.0
3	401	253	248	251.0	9.7	-52.8	334.4	Walderhaug et al. (2005) from Cocks and Torsvik... Gurevitch et al. (2004) from Cocks and Torsvik... GPDB3486, Kravchinsky et al. (2002) from Cocks... Pavlov and Gallet (1996) from Cocks and Torsvik... Pisarevsky et al. (2006) from Cocks and Torsvik... GPDB1991, Davydov and Kravchinsky (1973)	65.00 59.48 74.99 56.6 56.6 50.5	56.2 52.8 56.6 56.6 56.6 50.5	146.0 154.4 127.9 121.4 121.4 170.0
4	401	253	248	251.0	2.2	-56.6	307.9	Walderhaug et al. (2005) from Cocks and Torsvik... Gurevitch et al. (2004) from Cocks and Torsvik... GPDB3486, Kravchinsky et al. (2002) from Cocks... Pavlov and Gallet (1996) from Cocks and Torsvik... Pisarevsky et al. (2006) from Cocks and Torsvik... GPDB1991, Davydov and Kravchinsky (1973)	65.00 59.48 74.99 56.6 56.6 50.5	56.2 52.8 56.6 56.6 56.6 50.5	146.0 154.4 127.9 121.4 121.4 170.0
5	401	285	265	275.0	8.6	-50.5	301.4	Walderhaug et al. (2005) from Cocks and Torsvik... Gurevitch et al. (2004) from Cocks and Torsvik... GPDB3486, Kravchinsky et al. (2002) from Cocks... Pavlov and Gallet (1996) from Cocks and Torsvik... Pisarevsky et al. (2006) from Cocks and Torsvik... GPDB1991, Davydov and Kravchinsky (1973)	65.00 59.48 74.99 56.6 56.6 50.5	56.2 52.8 56.6 56.6 56.6 50.5	146.0 154.4 127.9 121.4 121.4 170.0
6	401	363	290	326.5	1.3	-21.0	350.0	Walderhaug et al. (2005) from Cocks and Torsvik... Gurevitch et al. (2004) from Cocks and Torsvik... GPDB3486, Kravchinsky et al. (2002) from Cocks... Pavlov and Gallet (1996) from Cocks and Torsvik... Pisarevsky et al. (2006) from Cocks and Torsvik... GPDB1991, Davydov and Kravchinsky (1973)	65.00 59.48 74.99 56.6 56.6 50.5	56.2 52.8 56.6 56.6 56.6 50.5	146.0 154.4 127.9 121.4 121.4 170.0
7	401	352	332	342.0	17.0	-16.0	295.0	GPDB1986, Kamyshneva (1971)	53.14	16.0	115.0
8	401	348	340	344.0	5.8	-25.2	320.0	GPDB3041, Zhitkov et al. (1994)	51.71	25.2	140.0
9	401	377	350	360.0	8.9	-11.1	329.7	GPDB3486, Kravchinsky et al. (2002) from Cocks... Pavlov and Gallet (1996) from Cocks and Torsvik... GPDB3486, Kravchinsky et al. (2002)	34.89	11.1	149.7
10	401	377	350	363.5	10.1	-27.8	339.9	GPDB3486, Kravchinsky et al. (2002)	42.02	27.8	159.9
11	401	377	350	363.5	11.9	-22.8	339.4	GPDB3486, Kravchinsky et al. (2002)	38.64	22.8	159.4
12	401	391	363	377.0	5.0	-13.0	302.0	GPDB1997, Kamyshneva (1975)	48.52	13.0	122.0
13	410	430	397	413.5	3.2	8.2	292.0	Powerman et al. (2013)	29.65	-8.2	112.0
14	401	443	423	433.0	4.6	19.0	308.0	Shatsillo et al. (2007) from Cocks and Torsvik... Powerman et al. (2013)	16.13	-19.0	128.0
15	410	444	423	433.5	4.4	18.4	302.7	Smethurst et al. (1998) from Cocks and Torsvik... Powerman et al. (2013)	17.92	-18.4	122.7
16	401	454	424	439.0	8.0	14.0	304.0	Smethurst et al. (1998) from Cocks and Torsvik... Powerman et al. (2013)	21.93	-14.0	124.0
17	401	460	440	450.0	17.3	19.4	315.3	Smethurst et al. (1998) from Cocks and Torsvik... Powerman et al. (2013)	13.66	-19.4	135.3
18	410	461	443	452.0	5.1	27.5	322.0	Powerman et al. (2013)	0.11	-27.5	152.0
19	401	464	458	461.0	2.5	22.8	334.2	GPDB3473, Iosifidi et al. (1999) from Cocks an... GPDB3473, Iosifidi et al. (1999) from Cocks an... Smethurst et al. (1998) from Cocks and Torsvik... Powerman et al. (2013)	3.31	-22.8	154.2
20	401	464	458	461.0	5.1	22.1	324.9	GPDB3473, Iosifidi et al. (1999) from Cocks an... Smethurst et al. (1998) from Cocks and Torsvik... Powerman et al. (2013)	7.79	-22.1	144.9
21	401	473	453	463.0	4.0	23.0	338.0	Smethurst et al. (1998) from Cocks and Torsvik... Powerman et al. (2013)	1.41	-23.0	158.0
22	401	470	464	467.0	3.2	30.9	332.7	GPDB3448 Gallet and Pavlov (1998) from Cocks a... Smethurst et al. (1998) from Cocks and Torsvik... Powerman et al. (2013)	-3.18	-30.9	152.7
23	401	478	458	468.0	3.1	24.4	316.0	Smethurst et al. (1998) from Cocks and Torsvik... Powerman et al. (2013)	-3.64	-24.4	166.0
24	401	479	459	469.0	4.0	30.0	337.0	Smethurst et al. (1998) from Cocks and Torsvik... Powerman et al. (2013)	-4.19	-30.0	157.0
25	401	480	460	470.0	9.0	17.9	342.8	Smethurst et al. (1998) from Cocks and Torsvik... Powerman et al. (2013)	3.43	-17.9	162.8
26	401	488	468	478.0	2.2	33.9	333.7	Smethurst et al. (1998) from Cocks and Torsvik... Powerman et al. (2013)	-5.44	-33.9	151.7
27	401	495	470	482.5	5.8	36.2	338.3	GPDB3474, Suroki et al. (1999) from Cocks and ... Smethurst et al. (1998) from Cocks and Torsvik... Powerman et al. (2013)	-10.30	-36.2	158.8
28	401	493	473	483.0	9.0	40.0	318.0	Smethurst et al. (1998) from Cocks and Torsvik... Powerman et al. (2013)	-6.50	-40.0	138.0
29	401	495	485	490.0	4.9	35.2	307.2	GPDB3448, Gallet and Pavlov (1998) from Cocks ... Smethurst et al. (1998) from Cocks and Torsvik... Powerman et al. (2013)	0.65	-35.2	127.2
30	401	495	485	490.0	2.3	41.9	315.8	GPDB3192, Pavlov and Gallet (1998) from Cocks ... Smethurst et al. (1998) from Cocks and Torsvik... Powerman et al. (2013)	-7.71	-41.9	135.8
31	401	510	490	500.0	6.0	37.0	318.0	Smethurst et al. (1998) from Cocks and Torsvik... Powerman et al. (2013)	-3.69	-37.0	138.0
32	401	505	495	503.0	3.0	36.1	310.7	GPDB3192, Pavlov and Gallet (1998) from Cocks ... Smethurst et al. (1998) from Cocks and Torsvik... Powerman et al. (2013)	-0.97	-36.1	130.7
33	401	518	495	506.5	4.5	32.6	333.8	GPDB3472, Rodionov et al. (1998) from Cocks an... Smethurst et al. (1998) from Cocks and Torsvik... Powerman et al. (2013)	-5.12	-32.6	153.8
34	401	514	500	507.0	2.6	43.7	320.5	GPDB3537, Gallet et al. (2003) from Cocks and ... Smethurst et al. (1998) from Cocks and Torsvik... Powerman et al. (2013)	-10.62	-43.7	140.5
35	401	518	505	511.5	4.6	36.4	319.6	GPDB3164, Pisarevsky et al. (1997) from Cocks ... Smethurst et al. (1998) from Cocks and Torsvik... Powerman et al. (2013)	-3.59	-36.4	139.6
36	401	520	510	515.0	5.1	53.3	315.0	GPDB3537, Gallet et al. (2003) from Cocks and ... Smethurst et al. (1998) from Cocks and Torsvik... Powerman et al. (2013)	-18.26	-53.3	135.0
37	401	535	518	526.5	6.8	44.8	338.7	GPDB3164, Pisarevsky et al. (1997) from Cocks ... Smethurst et al. (1998) from Cocks and Torsvik... Powerman et al. (2013)	-17.58	-44.8	158.7
38	401	538	518	528.0	7.0	32.0	317.0	Smethurst et al. (1998) from Cocks and Torsvik... Powerman et al. (2013)	-1.28	-32.0	137.0
39	401	545	525	535.0	6.2	16.6	244.5	GPDB1627, Kirschvink and Rozanov (1984) from C... GPDB3164, Pisarevsky et al. (1997) from Cocks ...	13.73	-16.6	64.5
40	401	545	535	540.0	12.8	37.6	345.0	GPDB3164, Pisarevsky et al. (1997) from Cocks ...	-14.15	-37.6	165.0

3.1.2 North China

We first load the paleomagnetic data for North China compiled in Cocks and Torsvik (2013).

We also add some additional poles from North China that were not included in Cocks and Torsvik (2013) including a compilation of data from Huang et al. (1999) and additional poles from Embleton et al. (1996), Huang et al. (2001), and Doh and Piper (1994).

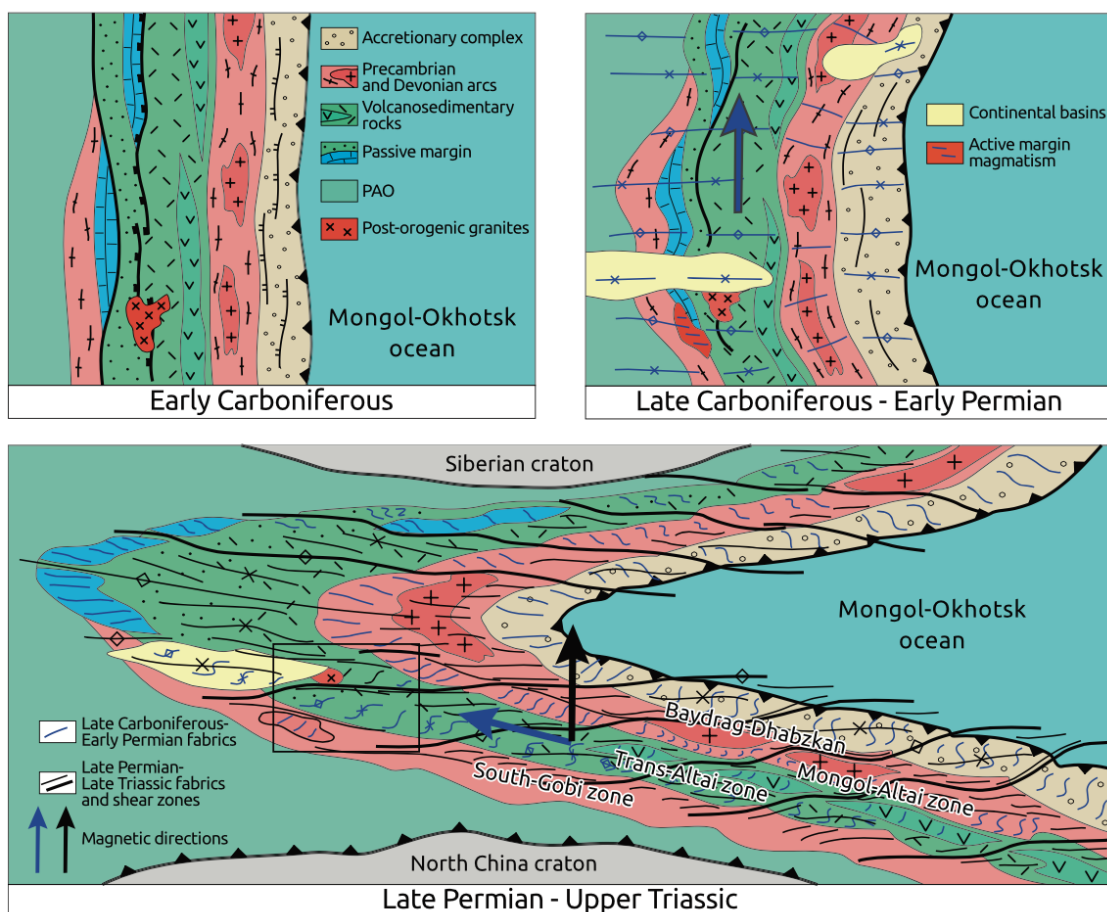
Out [112] :



	high_age	low_age	median_age	A95	PLat	PLon	References	PaleoLat	
0	88	68	78.0	5.8	79.7	170.8	see Van der Voo et al. (2015)	46.15	
1	98	78	88.0	5.3	81.1	294.5	see Van der Voo et al. (2015)	33.14	
2	110	90	100.0	4.7	70.6	156.7	see Van der Voo et al. (2015)	52.87	
3	123	103	113.0	5.2	76.8	192.1	see Van der Voo et al. (2015)	42.21	
4	126	106	116.0	4.6	83.6	172.3	see Van der Voo et al. (2015)	44.60	
5	128	108	118.0	5.9	75.2	147.7	see Van der Voo et al. (2015)	52.66	
6	128	108	118.0	12.2	69.0	200.7	see Van der Voo et al. (2015)	38.08	
7	131	111	121.0	3.0	84.8	30.2	see Van der Voo et al. (2015)	42.80	
8	131	111	121.0	6.5	82.7	159.6	see Van der Voo et al. (2015)	46.36	
9	138	118	128.0	6.8	73.9	153.6	see Van der Voo et al. (2015)	52.22	
10	165	145	155.0	6.8	59.9	240.3	see Van der Voo et al. (2015)	19.45	
11	165	145	145	155.0	7.9	72.8	180.3	see Van der Voo et al. (2015)	45.21
12	165	145	155.0	5.9	74.9	175.4	see Van der Voo et al. (2015)	46.35	
13	165	145	155.0	6.9	78.0	166.8	see Van der Voo et al. (2015)	47.46	
14	165	145	155.0	5.7	70.7	162.2	see Van der Voo et al. (2015)	51.14	
15	170	150	160.0	6.6	68.7	159.1	see Van der Voo et al. (2015)	52.80	
16	179	159	169.0	8.3	71.8	148.2	see Van der Voo et al. (2015)	54.64	
17	179	159	159	169.0	6.4	78.9	186.6	see Van der Voo et al. (2015)	37.49
18	179	159	169.0	4.5	78.1	175.2	see Van der Voo et al. (2015)	45.77	
19	198	178	188.0	6.8	84.0	112.9	see Van der Voo et al. (2015)	47.98	
20	198	178	188.0	5.5	84.4	98.6	see Van der Voo et al. (2015)	47.50	
21	235	208	221.5	5.8	70.9	49.8	see Van der Voo et al. (2015)	49.18	
22	235	208	221.5	3.8	65.6	36.1	see Van der Voo et al. (2015)	44.40	
23	241	235	238.0	4.0	64.7	22.1	see Van der Voo et al. (2015)	38.47	
24	241	235	238.0	3.1	52.8	36.6	see Van der Voo et al. (2015)	41.98	
25	241	235	238.0	3.9	52.2	46.9	see Van der Voo et al. (2015)	47.89	
26	245	241	243.0	6.6	55.1	359.9	see Van der Voo et al. (2015)	24.18	
27	251	245	248.0	3.8	67.7	37.5	see Van der Voo et al. (2015)	34.25	
28	251	245	248.0	4.8	55.7	19.8	see Van der Voo et al. (2015)	33.96	
29	261	251	256.0	8.9	64.7	27.4	see Van der Voo et al. (2015)	40.64	
30	261	251	256.0	6.9	48.8	5.6	see Van der Voo et al. (2015)	22.96	
31	261	251	256.0	4.0	52.9	7.4	see Van der Voo et al. (2015)	26.33	
32	261	251	256.0	6.9	42.0	9.5	see Van der Voo et al. (2015)	20.89	
33	270	256	263.0	12.2	20.9	1.4	GPDDB3086, Embbleton et al. (1996)	1.65	
34	303	295	299.0	16.7	33.3	10.2	GPDDB3468, Huang et al. (2001)	15.80	
35	320	307	313.5	7.2	44.6	335.7	GPDDB2734, Doh and Piper (1994)	6.14	
36	350	321	335.5	6.2	10.5	14.0	GPDDB3468, Huang et al. (2001)	3.34	
37	416	360	388.0	8.8	34.2	228.7	see Huang et al. (1999)	4.10	
38	444	416	430.0	8.2	26.2	228.4	see Huang et al. (1999)	-1.83	
39	488	444	466.0	12.3	28.8	310.9	see Huang et al. (1999)	-16.37	
40	472	461	466.5	7.0	31.5	327.7	Huang et al. (1999)	-8.33	
41	472	461	466.5	10.6	43.2	332.5	see Huang et al. (1999)	3.73	
42	472	461	466.5	9.2	27.9	310.4	see Huang et al. (1999)	-17.36	
43	488	472	480.0	8.5	37.4	324.3	Huang et al. (1999)	-4.32	
44	488	472	494.5	5.4	31.7	329.6	Huang et al. (1999)	-7.38	
45	513	501	507.0	5.5	37.0	326.7	Huang et al. (1999)	-3.84	
46	542	513	527.5	6.5	18.5	341.9	Huang et al. (1999)	-12.29	
47	542	513	527.5	12.4	21.2	335.2	see Huang et al. (1999)	-13.74	
48	542	513	527.5	9.9	15.0	298.6	see Huang et al. (1999)	-32.32	
49	542	513	527.5	8.9	26.8	334.5	see Huang et al. (1999)	-9.39	

3.1.3 Mongolia pole compilation

Edel et al. (2014) published paleomagnetic data from 12 sites in the Trans-Altai and South Gobi zones. This work identified magnetic overprint directions for which a variety of arguments are made as to their temporal relationship. The progression of directions as interpreted by the authors leads to an appreciable change in magnetic declination from overprints interpreted to be Middle–Late Carboniferous in age to magnetizations that are interpreted to be Permian in age. The authors propose that this declination change is the result of vertical axis rotation associated with oroclinal bending of a Mongolian ribbon continent (an illustration of this model shown below from that paper).



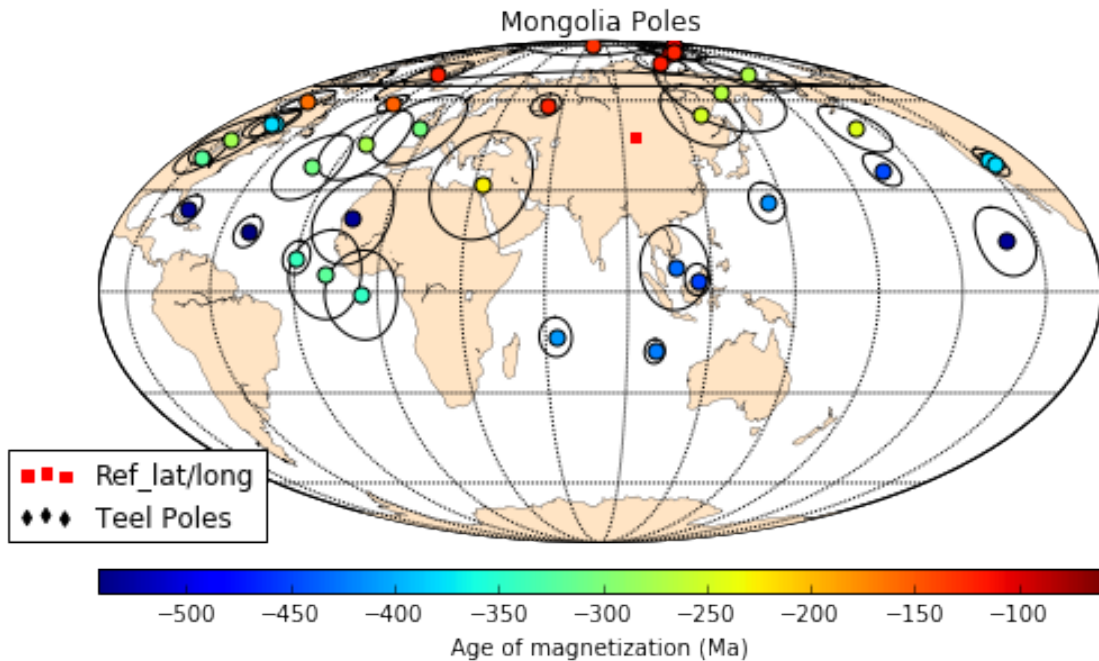
We import paleomagnetic data that have been compiled for Mongolia and some of the surrounding terranes between Siberia and North China and assigned them to established terranes pertinent to this study.

Out [115] :

Calculate paleolatitudes for the Mongolia poles, considering that many may have experienced horizontal-axis rotations during the formation of the COAB and possibly earlier.

terrane	high_	low_	age	median_	age	A95	PLat	PLat	Reference	Palcolat
0	Zavkhan	Baidrag	105	92	98.5	3.9	81.1	165.7	van Hinsbergen et al. (2008)	49.39
1	Zavkhan	Baidrag	146	65	105.5	21.4	86.9	252.8	GPDDB2443, Pruner (1992)	44.23
2	Zavkhan	Baidrag	124	92	108.0	2.5	80.8	158.4	van Hinsbergen et al. (2008)	50.58
3	Zavkhan	Baidrag	119	115	117.0	4.9	75.6	132.3	van Hinsbergen et al. (2008)	57.66
4	greater	Amuria	130	110	120.0	5.2	70.8	322.4	Cogne et al. (2005)	32.63
5	greater	Amuria	145	97	121.0	4.2	58.3	171.0	Halim et al. (1998)	61.51
6	greater	Amuria	125	118	121.5	4.3	82.0	172.3	van Hinsbergen et al. (2008)	48.32
7	greater	Amuria	133	125	129.0	7.4	86.8	61.8	Cogne et al. (2005)	49.73
8	greater	Amuria	161	145	153.0	3.1	58.9	327.3	Cogne et al. (2005)	24.23
9	greater	Amuria	176	145	160.5	4.2	59.6	279.0	Kravchinsky et al. (2002)	16.74
10	greater	Amuria	245	208	226.5	16.8	32.0	322.7	GPDDB2443, Pruner (1992)	40.78
11	southern	terrane	260	228	244.0	8.0	50.0	201.0	Edel et al. (2014)	26.32
12	Zavkhan	Baidrag	260	240	250.0	11.0	55.0	131.3	Kovalenko (2010)	66.39
13	greater	Amuria	271	260	265.5	14.4	63.1	151.0	Kravchinsky et al. (2002)	55.81
14	greater	Amuria	290	256	273.0	11.6	44.8	335.1	GPDDB2443, Pruner (1992)	15.82
15	southern	terrane	310	245	277.5	8.0	46.0	273.0	Edel et al. (2014)	3.12
16	southern	terrane	300	240	270.0	7.8	71.0	188.0	Kovalenko (2010)	43.04
17	Zavkhan	Baidrag	323	290	306.5	10.4	37.5	320.1	GPDDB2443, Pruner (1992)	3.57
18	southern	terrane	363	323	343.0	13.0	-1.0	354.1	GPDDB3045, Pechersky and Didenko (1995)	-8.39
19	southern	terrane	391	363	377.0	3.4	39.9	244.3	GPDDB3045, Pechersky and Didenko (1995)	1.30
20	southern	terrane	391	363	377.0	4.6	51.7	282.7	GPDDB3045, Pechersky and Didenko (1995)	9.00
21	southern	terrane	391	363	377.0	3.5	38.0	244.0	GPDDB2594, Grishin et al. (1991)	-0.40
22	southern	terrane	391	363	377.0	5.1	52.0	280.0	GPDDB2594, Grishin et al. (1991)	9.18
23	southern	terrane	363	245	304.0	11.9	50.0	354.0	GPDDB2594, Grishin et al. (1991)	28.35
24	southern	terrane	340	299	319.5	13.0	5.0	341.0	Edel et al. (2014)	-12.48
25	Zavkhan	Baidrag	440	200	320.5	5.6	40.8	269.4	This study	-1.94
26	southern	terrane	360	320	340.0	4.9	10.0	330.0	Kovalenko (2010)	-15.13
27	Lake	Zone	423	397	410.0	5.8	-13.3	63.7	Bachtadse et al. (2000)	23.28
28	Lake	Zone	428	397	412.5	6.1	26.3	144.0	Bachtadse et al. (2000)	46.72
29	Lake	Zone	428	416	422.0	3.6	-17.5	100.1	Bachtadse et al. (2000)	25.26
30	Zavkhan	Baidrag	450	410	430.0	12.3	7.0	106.7	Kravchinsky (2010)	48.74
31	Zavkhan	Baidrag	449	443	446.0	5.2	36.5	196.0	This study	19.57
32	Zavkhan	Baidrag	542	360	451.0	4.6	3.5	114.9	Evans et al. (1996)	43.25
33	Zavkhan	Baidrag	545	518	531.5	13.5	21.4	347.1	Kravchinsky (2001)	3.93
34	Zavkhan	Baidrag	545	518	531.5	10.1	14.7	228.6	GPDDB3045, Pechersky and Didenko (1995)	-15.37
35	Zavkhan	Baidrag	545	518	531.5	4.4	24.1	283.3	GPDDB3045, Pechersky and Didenko (1995)	-18.44
36	Zavkhan	Baidrag	650	518	584.0	4.7	17.6	309.7	GPDDB3045, Pechersky and Didenko (1995)	-18.32
37	Zavkhan	Baidrag	650	518	584.0	5.4	22.6	285.6	GPDDB3045, Pechersky and Didenko (1995)	-19.69

```
/Users/taylorkilian/Library/Enthought/Canopy_64bit/User/lib/python2.7/site-packages/matplotlib/a
warnings.warn("No labelled objects found. "
```



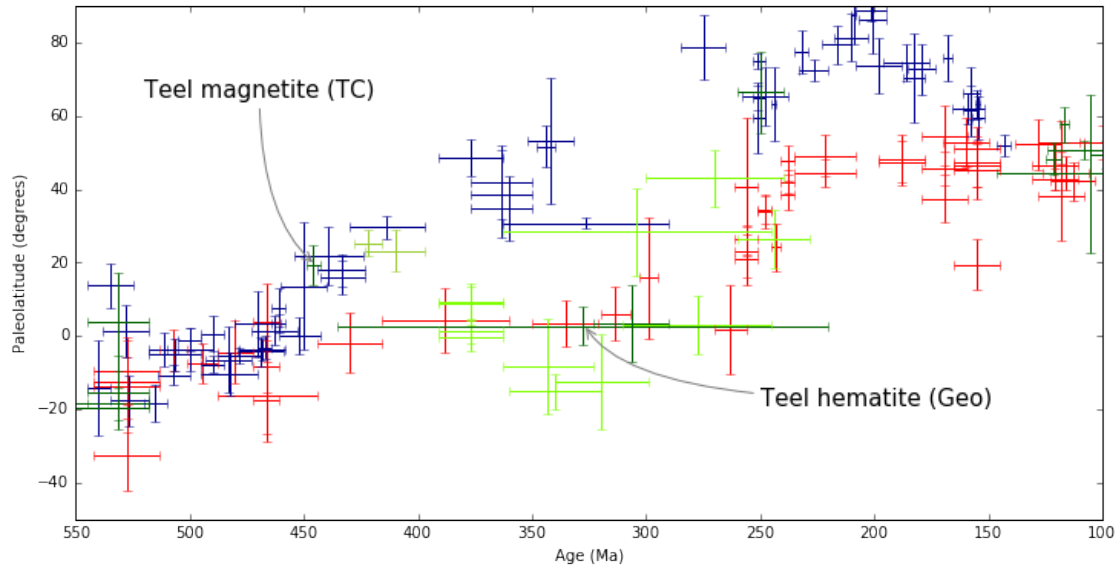
3.2 Paleolatitude diagram

We plot the data from Siberia, North China, and Mongolia (from Zavkhan, Baidrag, Lake Zone, and other southern terranes) on a paleolatitude versus time plot. The paleolatitudes given for each block are for specific reference points on each terrane. For Mongolia, the site of the Teel Formation (95.38°N , 47.1°E). For Siberia, coordinates at the southern tip of the craton (51.7°N , 103.5°E) are given seeing as this would be the proposed conjugate margin for Mongolia. For North China, a reference point on the northern margin (42°N , 109°E) is given to represent the alternative conjugate margin that would have shared similar paleolatitudes with Mongolia if they were attached.

There are a handful of Mongolian poles that we exclude because of wide age uncertainties or lack of statistical robustness. The Bachtadse et al. (2000) component B pole is excluded because of the small number or samples used to calculate the mean direction (25 samples; unblocking temperatures of $270\text{--}420^{\circ}\text{C}$); it is very similar to two Levashova (2010) directions which may be overprints (see below). The Evans et al. (1996) Bayan-Gol pole was superseded by results from Kravchinsky (2001) and may be a pre-folding overprint, given the increase in precision after tilt correction. The Kravchinsky et al. (2010) pole, that they call a remagnetization, has a very uncertain age and is not tilt-corrected, therefore we see it as unreliable for a paleolatitude estimate; the mean only originates from 6 sites, too. The Kovalenko (2010) pole from the granite at Hanbogd is excluded because it is only from one site and is in the Trans-Altai zone, which is severely affected by early Triassic

deformation along the Gobi-Tienshan fault (Lehmann et al., 2010). The “Mongolian sediments and volcanics, Gurvan-Sayhan Range, post-folding” pole from Grishin et al. (1991) (also discussed in Pechersky and Didenko (1995)) is not included because it is likely underaveraged (only from one site) and because of its large age uncertainty; it is also a post-folding remanence.

<matplotlib.figure.Figure at 0x118489e10>



4 Regional overprints in Precambrian rocks

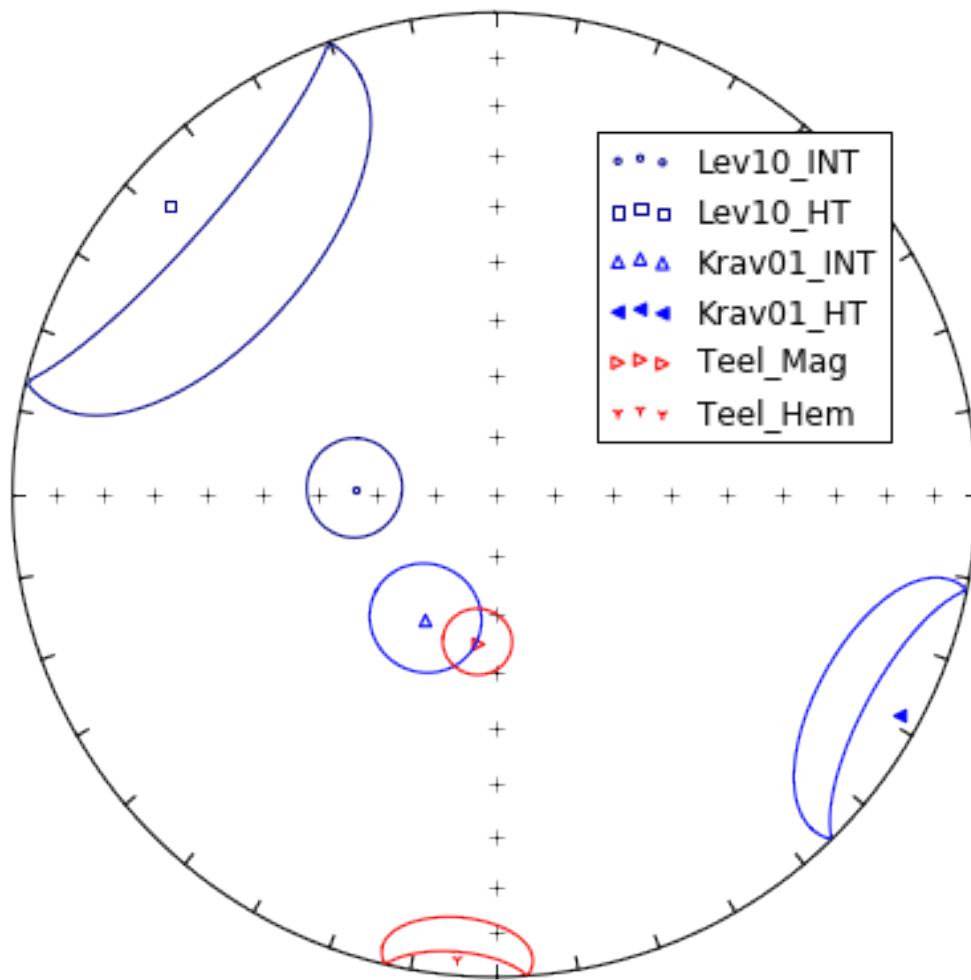
In order to understand the regional paleomagnetic directions, specifically possible overprints, we compare results from the Zavkhan block to see if there are dominant overprints that affected all rocks. These results are from Levashova et al. (2010), Kravchinsky et al. (2001), Evans et al. (1996), this study, and preliminary data from the Zavkhan volcanics. (Notes: B-G = Bayan-Gol; T-O = Tsagan-Olom)

Out [120] :

All directions are first plotted in geographic coordinates.

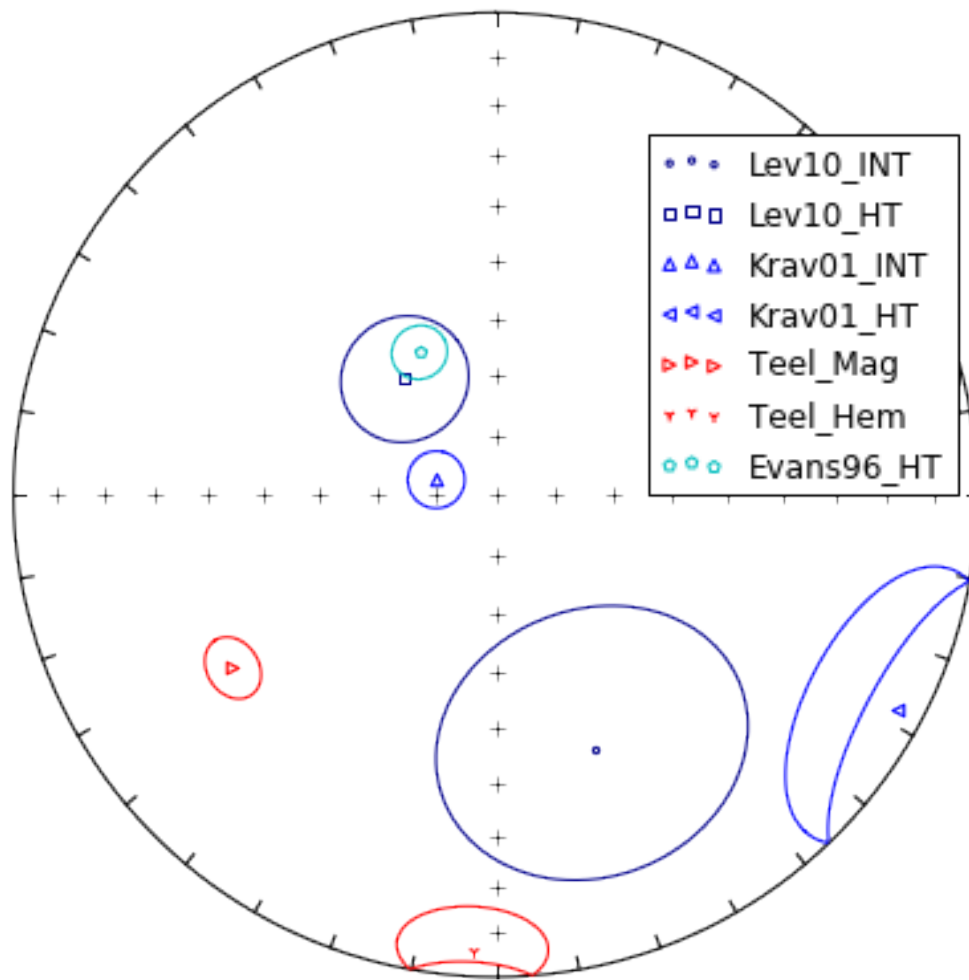
ID	N	k_geo	Dec_geo	Inc_geo	a95_geo	k_tc	Dec_tc	Inc_tc	a95_tc	comments
0	Lev10-INT	18	19.0	272.8	-66.2	8.2	3.0	158.7	-42.8	24.7 NaN
1	Levi0-HT	11	3.0	311.7	-11.0	30.1	19.0	321.9	-65.0	10.7 NaN
2	Levi1-INT	27	14.0	207.9	-30.6	7.8	6.0	210.4	-4.0	12.4 NaN
3	Levi1-HT	18	10.0	194.2	29.2	11.5	41.0	179.6	53.7	5.4 NaN
4	Krav01-LOW	10	59.7	4.1	70.9	6.3	96.8	181.2	85.6	4.9 data from both B-G and T-O
5	Krav01-INT	9	31.3	209.2	-66.0	9.3	117.6	284.3	-79.7	4.8 data from both B-G and T-O
6	Krav01-HT	6	14.9	118.5	5.3	17.9	13.3	118.3	-6.3	19.0 data from B-G
7	Teel_mag	23	29.1	186.6	-64.9	5.7	38.5	236.6	-35.0	4.9 NaN
8	Teel_hem	18	14.9	184.6	3.8	9.3	14.2	182.9	6.1	9.5 NaN
9	Evans-HT	193	NaN	NaN	NaN	5.8	331.9	-62.6	4.6	NaN
10	Z09_cg1_INT	20	32.3	200.7	-62.2	5.8	32.3	212.3	-5.8	5.8 NaN
11	Z104_cg1_INT	31	165.4	174.8	-61.7	2.0	165.2	61.9	-71.4	2.0 NaN

Overprint Directions - GEOGRAPHIC COORDS.



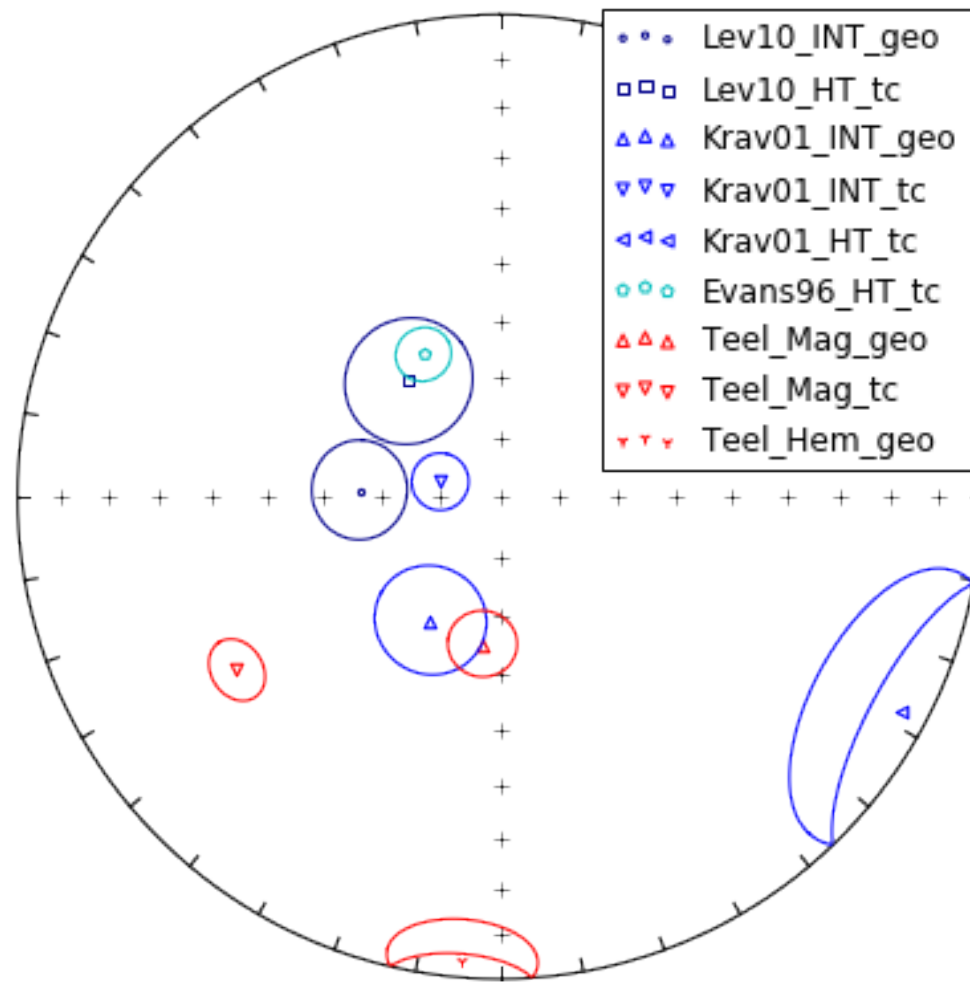
Then the overprint data are plotted in tilt-corrected coordinates.

Overprint Directions - Tilt-Corrected



Given geological and statistical paleomagnetic context (improvement during tilt correction) we create a plot of what we consider to be the overprint directions if they were acquired either before or after folding.

Overprint Directions - geographic/tilt-corrected



As stated in the main text, the Kravchinsky et al. (2001) intermediate component from late Neoproterozoic to early Cambrian in geographic coordinates is similar to the Teel magnetite component in geographic coordinates. It is possible that the Ordovician magmatism recorded in the Teel Formation basalts caused this overprint in older lithologies.

5 Data Repository References

Bachtadse, V., Pavlov, V. E., Kazansky, A. Y., and Tait, J. A., 2000, Siluro-Devonian paleomagnetic results from the Tuva Terrane (southern Siberia, Russia): implications for the paleogeography of Siberia: Journal of Geophysical Research: Solid Earth, vol. 105, pp. 13,509-13,518,

doi:10.1029/1999JB900429.

Cogne, J.-P., Kravchinsky, V. A., Halim, N., and Hankard, F., 2005, Late Jurassic-Early Cretaceous closure of the Mongol-Okhotsk Ocean demonstrated by new Mesozoic palaeomagnetic results from the Trans-Baikal area (SE Siberia): *Geophysical Journal International*, vol. 163, pp. 813-832, doi:10.1111/j.1365-246X.2005.02782.x.

Edel, J. B., Schulmann, K., Hanzl, P., and Lexa, O., 2014, Palaeomagnetic and structural constraints on 90° anticlockwise rotation in SW Mongolia during the Permo-Triassic: Implications for Altai oroclinal bending. Preliminary palaeomagnetic results: *Journal of Asian Earth Sciences*, vol. 94, pp. 157-171, doi:10.1016/j.jseaes.2014.07.039.

Evans, D. A., Zhuravlev, A. Y., Budney, C. J., and Kirschvink, J. L., 1996, Palaeomagnetism of the Bayan Gol Formation, western Mongolia: *Geological Magazine*, vol. 133, pp. 487-496.

Grishin, D., Didenko, A., Pechersky, D., and T.L., T., 1991, [Paleomagnetic study and petromagnetic study of structure and evolution of paleoceanic lithosphere (Phanerozoic ophiolites of Asia)] (in Russian), VNIGRI, Leningrad, Russia, pp. 135-149.

Halim, N., Kravchinsky, V., Gilder, S., Cogne, J.-P., Alexyutin, M., Sorokin, A., Courtillot, V., and Chen, Y., 1998, A palaeomagnetic study from the Mongol-Okhotsk region: rotated Early Cretaceous volcanics and remagnetized Mesozoic sediments: *Earth and Planetary Science Letters*, vol. 159, pp. 133-145, doi:10.1016/S0012-821X(98)00072-7.

Kovalenko, D., 2010, Paleomagnetism of Late Paleozoic, Mesozoic, and Cenozoic rocks in Mongolia: *Russian Geology and Geophysics*, vol. 51, pp. 387-403, doi:10.1016/j.rgg.2010.03.006.

Kravchinsky, V., Konstantinov, K., and Conge, J., 2001, Palaeomagnetic study of Vendian and Early Cambrian rocks of South Siberia and Central Mongolia: Was the Siberian platform assembled at this time?: *Precambrian Research*, vol. 110, pp. 61-92.

Kravchinsky, V. A., Cogne, J.-P., Harbert, W. P., and Kuzmin, M. I., 2002, Evolution of the Mongol-Okhotsk Ocean as constrained by new palaeomagnetic data from the Mongol-Okhotsk suture zone, Siberia: *Geophysical Journal International*, vol. 148, pp. 34-57.

Kravchinsky, V. A., Sklyarov, E. V., Gladkochub, D. P., and Harbert, W. P., 2010, Paleomagnetism of the Precambrian Eastern Sayan rocks: Implications for the Ediacaran-Early Cambrian paleogeography of the Tuva-Mongolian composite terrane: *Tectonophysics*, vol. 486, pp. 65-80, doi:10.1016/j.tecto.2010.02.010.

Pechersky, D. and Didenko, A., 1995, Paleo-Asian Ocean (in Russian): United Institute of Earth's Physics Publ., Moscow, 298 pp.

Pruner, P., 1992, Palaeomagnetism and palaeogeography of Mongolia from the Carboniferous to the Cretaceous - final report: *Physics of the Earth and Planetary Interiors*, vol. 70, pp. 169-177, doi:10.1016/0031-9201(92)90179-Y.

Van Hinsbergen, D. J. J., Straathof, G. B., Kuiper, K. F., Cunningham, W. D., and Wijbrans, J., 2008, No vertical axis rotations during Neogene transpressional orogeny in the NE Gobi Altai: coinciding Mongolian and Eurasian early Cretaceous apparent polar wander paths: *Geophysical Journal International*, vol. 173, pp. 105-126, doi:10.1111/j.1365-246X.2007.03712.x.